

FLUID EVOLUTION DURING BURIAL DIAGENESIS AND SUBSEQUENT OROGENETIC UPLIFT: THE LA VID GROUP (CANTABRIAN ZONE, NORTHERN SPAIN)

JOCHEN SCHNEIDER,^{1,*} RONALD J. BAKKER,² THILO BECHSTÄDT,¹ AND RALF LITKE³

¹Geological–Paleontological Institute, Ruprecht-Karls Universität, Im Neuenheimer Feld 234, D-69120 Heidelberg, Germany

²Department of Applied Geosciences and Geophysics, Mineralogy & Petrology, Montanuniversität, Peter Tunner Strasse 5, A-8700 Leoben, Austria

³Institute of Geology and Geochemistry of Petroleum and Coal, RWTH Aachen, Lochnerstrasse 4-20, D-52056 Aachen, Germany
e-mail: ronald.bakker@mu-leoben.at

ABSTRACT: The investigated section of the Lower Devonian La Vid Group (Cantabrian Zone, northern Spain) was deposited in a rifted-continental-margin setting, which in the Carboniferous evolved into a foreland basin, affected by Variscan thin-skinned folding and thrusting. Soon thereafter the originally linear orogenic belt underwent secondary curvature, forming the Variscan Ibero–Armorican Arc. This bending caused extension, crustal thinning, and strike-slip movements in the outer part of the orocline, to which the area of our investigation belongs. Subsequently the Variscan orogen subsided in Mesozoic and Cenozoic times, was covered by sediments of unknown thickness, and was affected by Alpidic tectonics. The Paleozoic Cantabrian Basin is an outcrop analogue for kilometer-scale differences in type and degree of porosity and cementation that can be expected in foreland basins of other areas as well.

Origin of cements and related fluids in the La Vid carbonates can be described by three distinct fluid-evolution mechanisms: local *in-situ* fluid generation, mixing of external with internally generated fluids, and incursion of exotic fluids. The oldest recorded fluid belongs to the basin stage in pre-Variscan times. Upward migration of an *in-situ* generated fluid from underlying organic-rich shales through iron-rich sandstones into the carbonates of the La Vid Group was accompanied by the precipitation of various Fe-carbonates in various stratigraphic positions of this succession. Among the cements are ferroan saddle dolomites with inclusions of solid bitumen in the lower part and mature petroleum in the upper part of the succession. Assuming a common origin of petroleum and aqueous fluid inclusions in the ferroan saddle dolomite, trapping conditions of 114 to 130°C and a pressure of about 38.5 to 40.5 MPa were determined; this corresponds to a burial depth of about 3850 to 4050 m.

The second important fluid event exhibits mixing of a low-salinity internally generated local fluid with an exotic high-salinity fluid of widespread occurrence. This fluid is attributed to the time of Variscan orogenesis, probably the formation of the Cantabrian orocline, based on several tectonic features occurring in the cements. Clear saddle dolomite precipitated during this fluid event in the dolostone unit of the La Vid Group only. These dolomites exhibit a distribution of zoned fluid inclusions from low salinity in the cores to high salinity in the outer parts of the crystals. Minimum trapping temperatures are 160 to 170°C at the core and temperatures of 110 to 120°C at the rim. Higher temperatures in the rim (up to 210°C) appear to have resulted from post-entrapment reequilibration (stretching) of the inclusions during Variscan deformation.

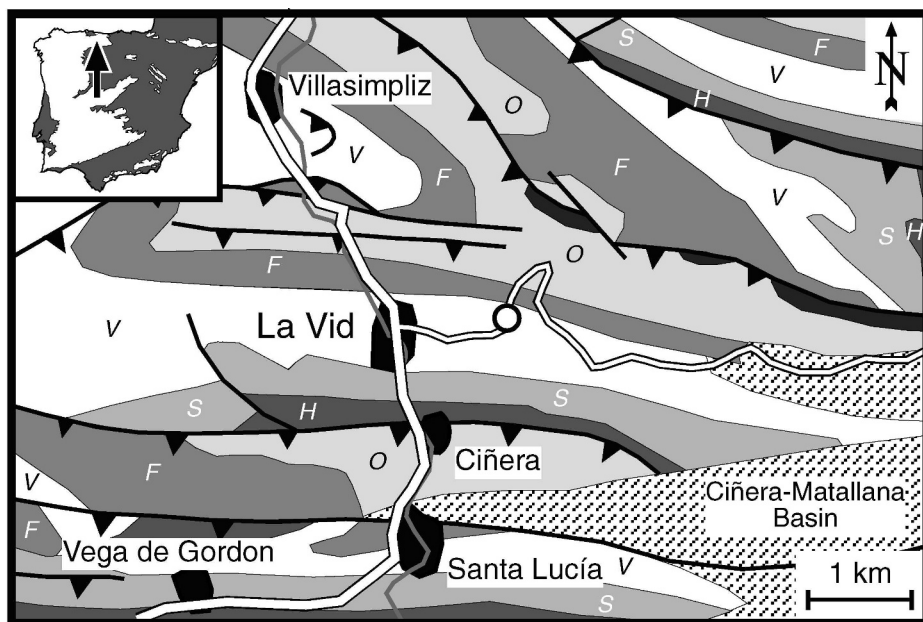
The last cementation phase was caused by a cool and oxidizing fluid, related to tectonic activity, most probably of Alpidic age. This fluid precipitated calcite, celestite, and kaolinite and recrystallized former Fe-carbonate cements to calcite and to Fe-oxyhydroxides. Fluid inclusions in celestite have low salinities, ruling out basinal brines and pointing to a meteoric or marine origin. Occurrences of these cements in various locations all over the Cantabrian Zone imply a large-scale fluid event.

INTRODUCTION

The Cantabrian Zone (northern Spain) is the outermost part of the Iberian Variscan orogen (Dallmeyer and Martínez-García 1990). Due to the low thermal overprint by diagenetic and low metamorphic conditions (e.g., Brime et al. 2001) this zone is an ideal study area for low-temperature events, which took place after deposition during burial of sediments. Reconstruction of pore-fluid properties and fluid-rock interactions is essential to unravel basin development and to further discriminate specific tectonic settings. For example, anisotropic features

like major fault zones are likely to be highly influenced by fluid flow and fluid-induced alterations. Until recently, fluids involved in diagenetic processes and the related thermal evolution of rocks in the Cantabrian Zone have been studied indirectly, mainly by means of isotope analyses (Immenhauser et al. 2002, Schneider et al. 2004a), illite crystallinity (Brime 1985, Keller and Krumm 1993), conodont alteration index (Raven and van der Pluijm 1986), vitrinite reflectance combined with the anisotropy of magnetic susceptibility (Frings et al. 2004), and isotope analyses combined with magnetic susceptibility (Schneider et al. 2004b). Fluid inclusions are regarded as remains of fluids present in the pore space during crystal growth (e.g., Samson et al. 2003). The abundance of fluid inclusions present in the investigated cements and the scarcity of

* Present address: Fesa e.V., Im Solar Info Center, D-79072 Freiburg, Germany



- Cambrian Lancara Fm.: Carbonates and dolomites
- Ordovician Oville & Barrios Fm.: Sandstones
- Silurian Formigoso & San Pedro Fm.: Shales and sandstones
- Devonian La Vid Group: Dolostones, limestones and shales
- Devonian Santa Lucia Fm.: Gray reef limestones
- Devonian Huergas Fm.: Shales and sandstones
- Stephanian rocks (undifferentiated)

- Thrust fault
- Fault

FIG. 1.—Schematic geological map of La Vid in the Somiedo-Correcillas Unit, along the national road from León to Oviedo (after Suárez et al. 1994). The open circle indicates the locality of the studied succession of the La Vid Group at the type section.

fluid-inclusion studies illustrate the deficiency in using these objects directly in modeling paleo-fluid properties and the thermal evolution of the sedimentary basin. Paniagua et al. (1993) studied fluid inclusions in quartz related to ore mineralizations in the Carboniferous. More recently, Grimmer (2001), Gasparrini (2003), Gasparrini et al. (2006a), Gasparrini et al. (2006b), Lapponi et al. (2004), and Lapponi et al. (2005) used fluid inclusions to characterize the nature of fluids and the thermal conditions in cements of overpressure breccias and epigenetic dolomites, respectively, both occurring in limestones of early Carboniferous age. Ayllón et al. (2003) investigated the thermal evolution of the Stephanian Ciñera-Matallana coal basin, mainly on the basis of fluid inclusions.

The aim of this study, based on the thesis of Schneider (2002), is to use fluid inclusion data directly to reconstruct the diagenetic history in a relatively undisturbed succession between major thrust zones in the Cantabrian Zone. Formation conditions of cements as well as the thermal evolution in the Lower Devonian La Vid Group in the type area (Fig. 1) are interpreted directly from fluid inclusion data. A conceptual model of diagenetic evolution is provided, which is based on a detailed cement stratigraphy. Local variations in the diagenetic history of the Cantabrian

Zone are illustrated with some examples, depending on lithology and burial differences.

The lower part of the La Vid Group was dolomitized in an early diagenetic stage (Keller and Grötsch 1990) shortly after deposition. All of the cements described in the present study postdate this early dolomitization event. Volumetrically important epigenetic dolomitizations, present a few kilometers farther north in Cambrian and Carboniferous rocks (Gasparrini 2003) Gasparrini et al. (2006a), Gasparrini et al. (2006b), Lapponi et al. (2004), and Lapponi et al. (2005) are absent in the study area (Fig. 1).

The Paleozoic Cantabrian Basin is a useful outcrop analogue for the type and degree of porosity and cementation that can be expected in buried foreland basins of other areas as well. Such small-scale variations might pose difficulties for hydrocarbon exploration and production in comparable settings. These differences are probably due to the heterogeneities of the aquifers in this structural setting, which is characterized by the development of a formerly rifted continental margin into a thin-skinned foreland fold-and-thrust belt, which then underwent oroclinal bending (formation of the Ibero-Armorican Arc).

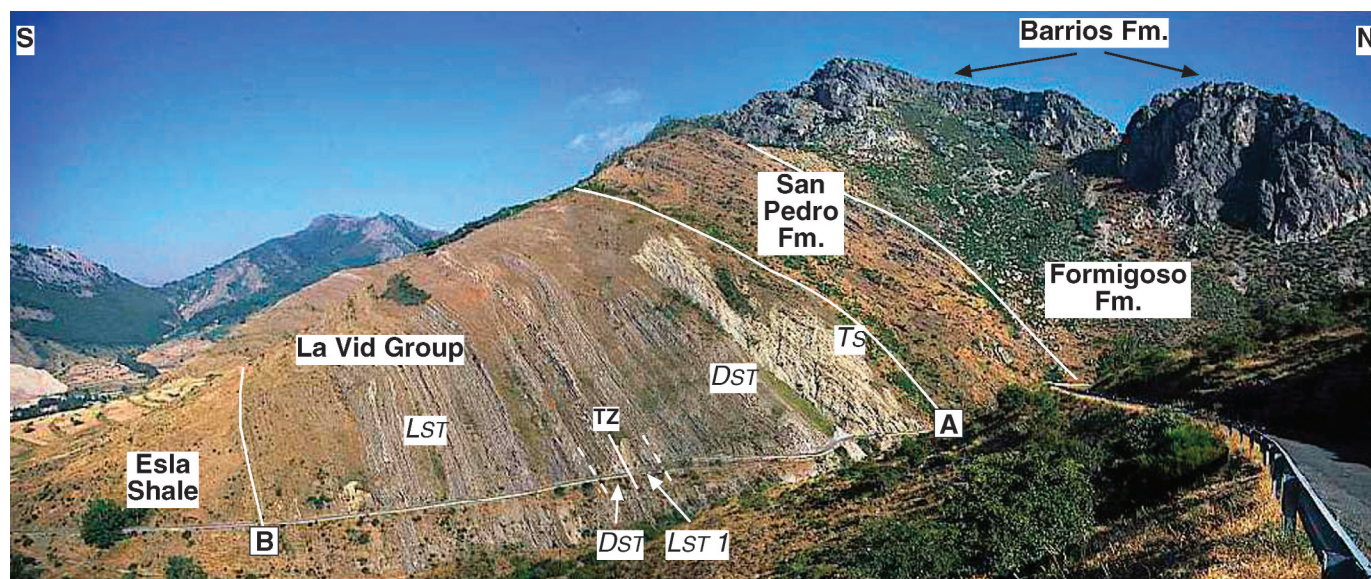


FIG. 2.—La Vid type section. Oldest rocks in the tilted succession occur in the farthest right of the picture. Here, Ordovician-age Barrios sandstones form the mountain ridge and are unconformably topped by a succession of formations including (from oldest to youngest) the shales of the Silurian Formigoso Fm., Fe sandstones of the San Pedro Fm., and Lower Devonian carbonates and shales of the La Vid Group. The La Vid Group (250 m from A to B) can be subdivided in the transitional sandstones (TS), the dolostones (DST), and limestones (LST) (see also Figure 3). The marked small-scaled thrust fault (TZ) is responsible for doubling of the succession.

GEOLOGICAL SETTING

Overlying a predominantly siliciclastic succession of Cambrian to Silurian age (Fig. 2), the Devonian La Vid Group represents the second Paleozoic carbonate interval and the beginning of thick carbonate sedimentation, which continued into the early Carboniferous. Cambrian and Ordovician terrigenous clastics are separated by a discontinuity from the overlying Silurian shales of the Formigoso Fm., which also contain organic-matter-rich layers (Evers 1967). The latter are overlain by Upper Silurian to Lower Devonian sandstones of the San Pedro Fm. (Evers 1967), prominent due to its reddish iron-rich layers at the base and top. “Transitional Sandstones” (TS in Fig. 3; Keller and Grötsch 1990) of Early Devonian age form an intermediate interval between San Pedro Fm. and overlying La Vid carbonates. Carbonate-cemented sandstones become more dominant upwards in these Transitional Sandstones, and the percentage of siliciclastic material decreases towards the overlying dolostones of the Abelgas Fm. of the La Vid Group (Keller and Grötsch 1990). This lower part of the La Vid succession comprises a series of dolostones (DST in Fig. 3). It is overlain by various facies types of limestone, which can be subdivided into three limestone units (Fig. 3): Limestone 1 (LST 1) comprises variable types of carbonate rocks from mudstones to grainstones with a few layers containing organic matter. Limestone 2 (LST 2) is predominantly composed of fine-grained wackestones to grainstones. Limestone 3 (LST 3), which is interbedded with shales, is characterized by coarse-grained crinoidal grainstones. This succession of the Abelgas Fm. grades into the overlying Esla shales, which are still of Early Devonian age (Keller and Grötsch 1990).

Structurally, the investigated section of the Lower Devonian La Vid Group (Fig. 1) at the type area belongs to the Somiedo–Correcillas Unit of the Cantabrian Zone. The La Vid Group was deposited in a rifted continental (“passive”) margin setting, which evolved during the Carboniferous into a foreland basin, affected by Variscan thin-skinned folding and thrusting of nappes from the hinterland to the west (Lotze 1945; Julivert 1971; Julivert and Marcos 1973; Pérez-Estaún et al. 1988; Pérez-Estaún and Bastida 1990; Veselovsky et al. in press). After nappe emplacement, the originally linear orogenic belt underwent secondary curvature, forming an orocline (Carey 1955). The Cantabrian Zone

represents the core of this Variscan Ibero–Armorican Arc. Recent paleomagnetic data point to a late Stephanian age (ca. 300 Ma) for this oroclinal bending (Van der Voo et al. 1997; Weil et al. 2000, 2001). The bending of the orogenic belt caused extension, crustal thinning, and strike-slip movements in the outer part of the orocline (which is the area of our investigation) and compression and strong crustal thickening in the inner part (Gutiérrez-Alonso et al. 2004). This process led to delamination of the thickened lithospheric root in the strongly compressed part. The delaminated lithosphere sank into the mantle and was displaced by hot upwelling asthenosphere (Gutiérrez-Alonso et al. 2004). The Variscan orogen of Northern Spain subsided in Mesozoic and Cenozoic time, was covered by sediments of unknown thickness and was subsequently affected by Alpidic tectonics. Variscan faults were partly reactivated during this Alpidic orogeny.

Internally, the investigated succession is relatively undeformed. Only a few minor thrust zones caused tectonic repetition, the most significant of which is displayed in Figure 2 (TZ), responsible for repeating of the upper part of the DST and the lower part of LST 1 (see also Fig. 3). The succession at the type section was tilted with an E–W trending orientation, dipping 69° north at the base (A in Fig. 2) to 59° north in the last layer at the top (B in Fig. 2).

SAMPLES AND METHODS

The investigated cements occur in molds, interparticle pore spaces, and veins. A total of 60 samples were taken over the investigated part of the succession (Fig. 3) for petrographic and fluid-inclusion analyses. Thin sections and thick sections were prepared for petrographic studies including cold cathodoluminescence technique, potassium ferricyanide staining (Dickson 1965), fluorescence analyses, microthermometry, micro-Raman spectroscopy, and scanning electron microscopy (SEM). Cathodoluminescence (CL) microscopy was performed on a CITL Cold Cathode Luminescence 8200 mk3 using a beam voltage of 18–20 kV and a beam current of about 550 mA.

Thin sections were examined for fluorescing inclusions by vertical UV illumination with a high-pressure mercury lamp (100 W). An UV filter

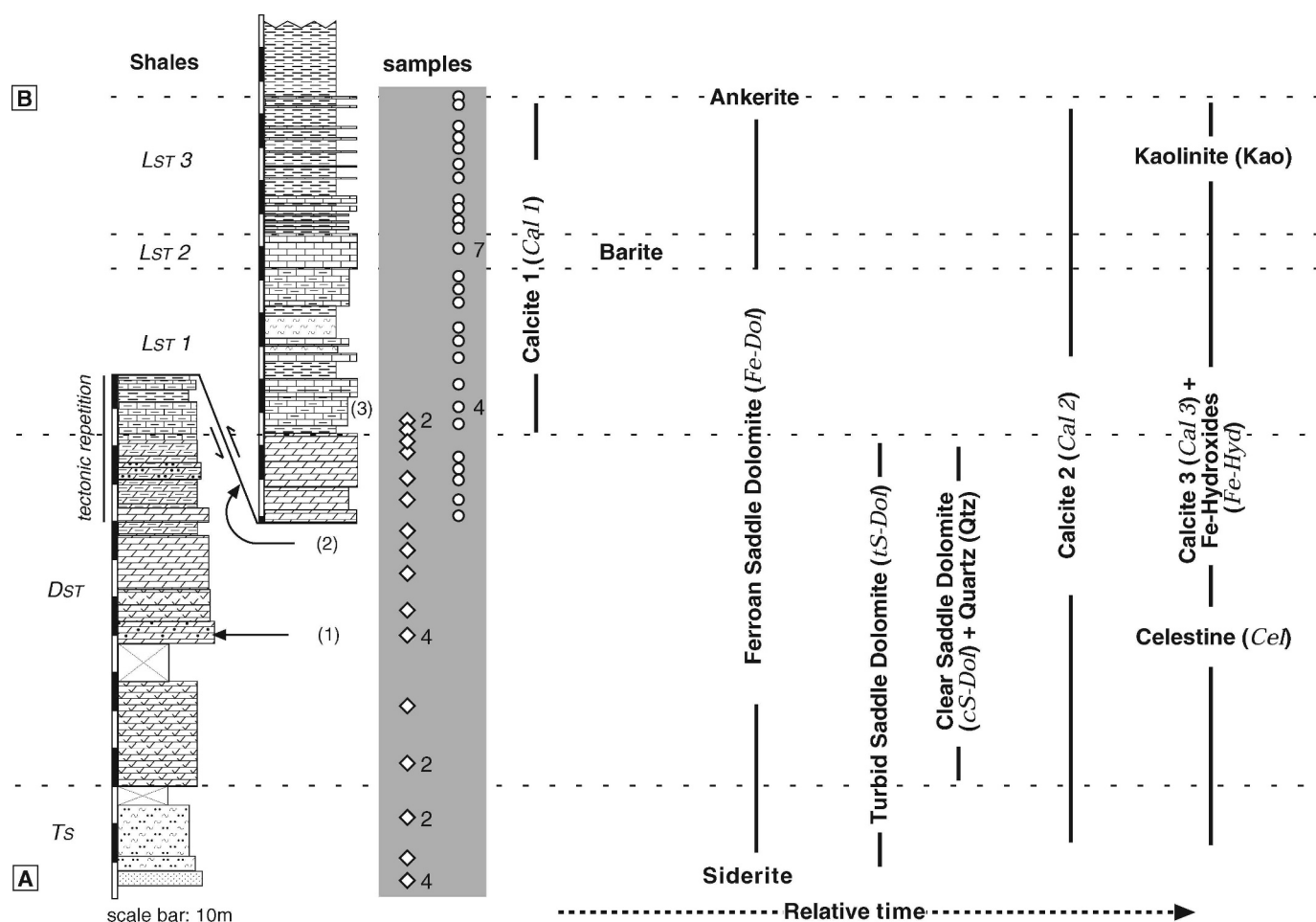


FIG. 3.—The stratigraphic succession (unpublished data, Z. Veselovsky, University of Heidelberg) of the La Vid Group with sample localities (numbers correspond to the amount of selected samples other than 1). The distribution of the observed cements are schematically illustrated (see text for further details). A and B correspond to the localities indicated in Figure 2. (1) Nodules with *Cal 3* and *Cel* occur in this horizon. (2) Veins with *Cal 3* in fault zone. (3) *Cal 1* and *Fe-Dol* blue-fluorescing oil inclusions in fossil molds. Bituminite occurs in the host rock.

(excitation filter BP 340–380 nm, barrier filter 430 nm) and a blue filter (excitation filter BP 420–490 nm, barrier filter 520 nm) were used.

For microthermometric investigations double-polished thick sections (100 to 150 μm) were prepared with a low-temperature technique. These rock slices were broken into small pieces and subsequently measured on a Linkham TMS 600 heating/cooling stage. The stage was calibrated with synthetic $\text{H}_2\text{O}-\text{CO}_2$ fluid inclusions, supplied by SYN-FLINC, at -56.6 , 0.0 , and 374.0°C , and the melting of AgNO_3 at 210°C . Mineral phases, gas phases, aqueous fluids and salt hydrates were analyzed with a LABRAM (Jobin Yvon GmbH) confocal Raman spectrometer with a green laser (532.2 nm excitation wavelength, 10 mW). Controlled low-temperature Raman measurements down to -190°C were obtained by using an attached Linkham TMS 600 stage (see also Dubessy et al. 1982; Bakker 2004).

For scanning electron microscopy (SEM) polished thin sections were coated with carbon in an argon atmosphere to generate a conductive layer. SEM investigations were performed on a LEO 440 with an EDX-apparatus (Oxford, Link Isis 300) at the Institute for Environmental Geochemistry, University of Heidelberg. The acceleration voltage was 20 kV.

Sr-isotope analyses of drilled host rock and cement samples were conducted at the University of Alberta, Canada, on Sr extracted from HCl solution using standard cation exchange procedures (Baadsgaard et

al. 1986). Ratios of $^{87}\text{Sr}/^{86}\text{Sr}$ were measured on a VG 354 thermal ionization mass spectrometer. Precision of individual runs was better than 0.00004. Repeated measurements of NBS SRM-987 gave a long-term laboratory average of $^{87}\text{Sr}/^{86}\text{Sr} = 0.710235$ throughout the course of this study.

CEMENT PETROGRAPHY

Cements in the La Vid Group occur in various stratigraphic positions (Fig. 3) and can be divided into three stages on the basis of petrographic characteristics, associated tectonic features and crosscutting relationships, as schematically illustrated in Figure 4: an early (Fig. 4A), an intermediate (Fig. 4B), and a late stage (Fig. 4C).

Early Stage

Cements belonging to this stage precipitated in most of the pore spaces (*LST 1*, *LST 2*, *LST 3*, *Ts*, for abbreviations see Fig. 3), cavities (*LST 2*, *DST*) and veins (*LST 2*, *DST*, *Ts*) of the different units. In *LST 1* to 3 fossil fragments are partially replaced with high-Mg calcite. Low-Mg calcite shells of brachiopods are non-luminescent and show no significant recrystallization features.

The first cement generation, calcite 1 (*Cal 1*), occurs directly on vein and cavity walls. White calcite crystals precipitated in veins as

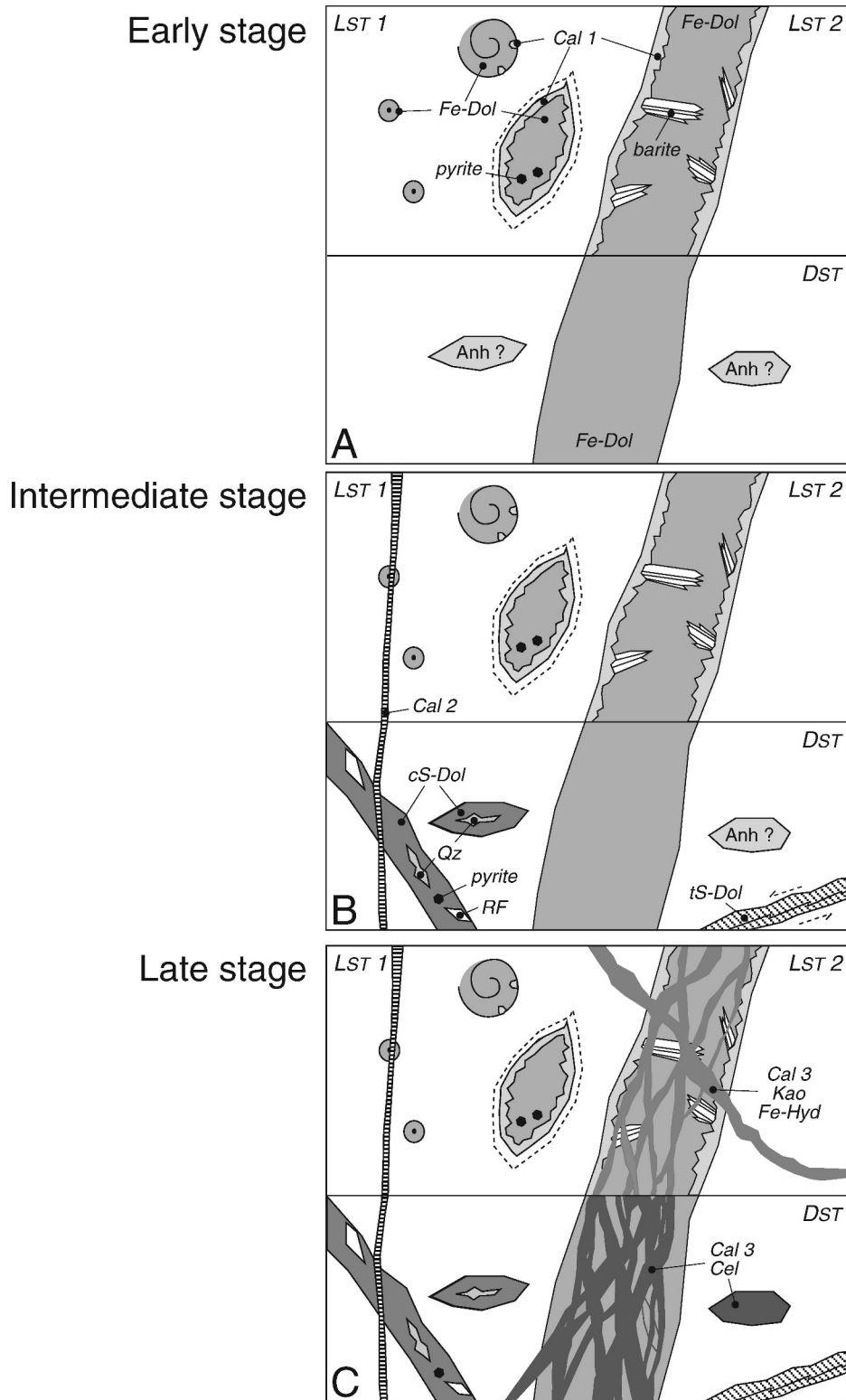
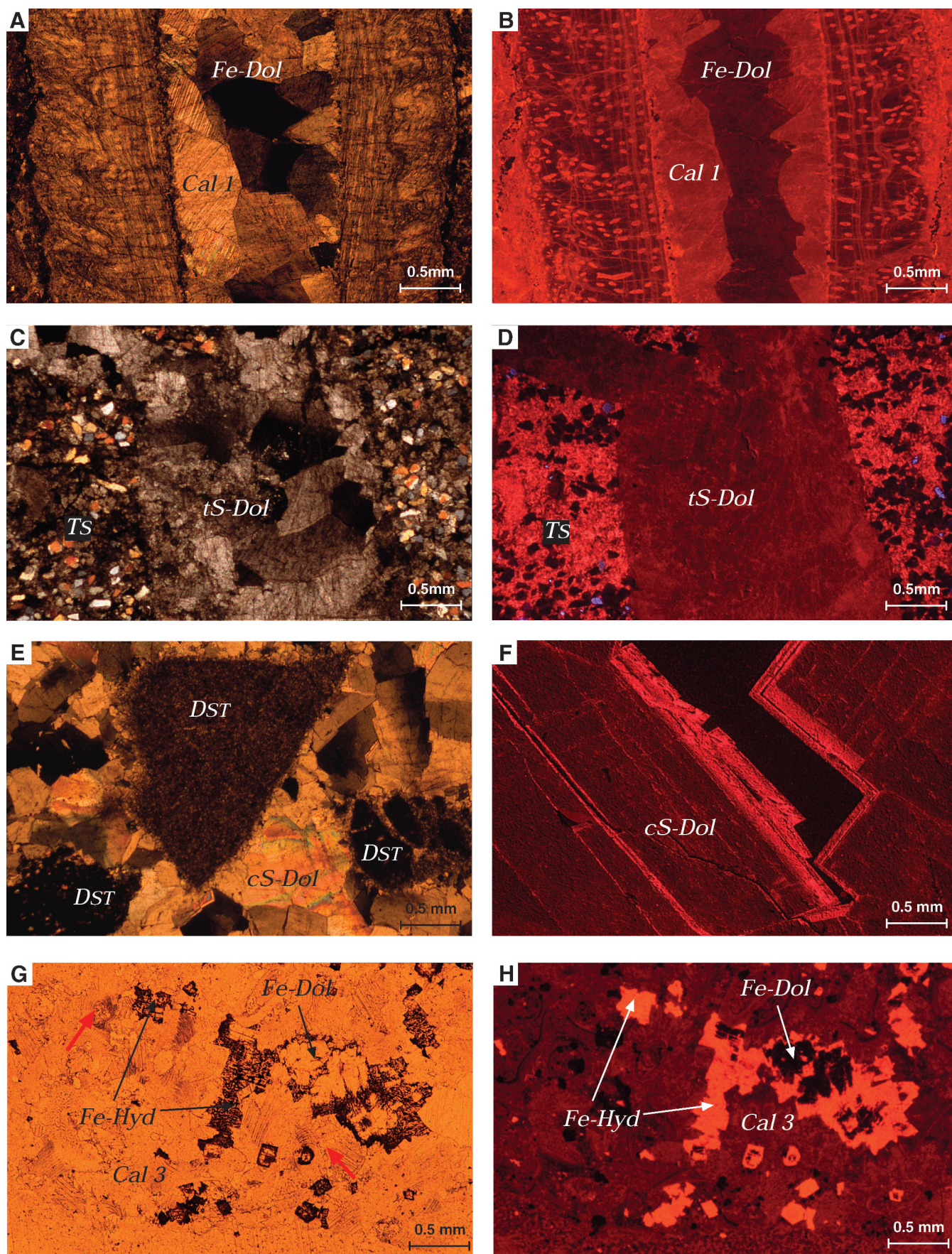


FIG. 4.—Schematic distribution of the different cement generations in the La Vid Group during the **A**) early, **B**) intermediate, and **C**) late stage. Illustrated are the dolostone (DST) and limestone units 1 and 2 (LST 1 and 2). Nodules within the DST were presumably filled with sulfates (Anh?). Cements occurring in the different stages are (A) calcite 1 (Cal 1), barite, ferroan saddle dolomite (Fe-Dol), pyrite; (B) turbid saddle dolomite (tS-Dol), clear saddle dolomite (cS-Dol with rock fragments, RF), quartz (Qz), pyrite, calcite 2 (Cal 2); and (C) calcite 3 (Cal 3), celestite (Cel), kaolinite (Kao), Fe-hydroxides (Fe-Hyd).

FIG. 5.—Microphotographs of Cal 1, Fe-Dol, tS-Dol, cS-Dol, and Cal 3 in cross-polarized light (A, C, E, and G) and cathodoluminescence (B, D, F, and H). **A, B**) Part of a punctate brachiopod in LST 1. The crystals of Fe-Dol are non-luminescent and show an undulatory extinction, whereas Cal 1 luminesces orange. **C, D**) A vein with tS-Dol having a red luminescence within the upper part of TS. **E**) Clear crystals of cS-Dol surround fragments of the dolomitic host rock DST. Sporadically the crystals show an undulatory extinction. **F**) cS-Dol is red luminescing with zonation to brighter colors towards an open cavities. **G, H**) Remnants of Fe-Dol, adjacent to Fe-hydroxide (Fe-Hyd) which is luminescing bright orange, and calcite (Cal 3) with an orange luminescence.



schematically illustrated in Figure 4A and on the inner rims of fossil shells (Fig. 5A, B). Bands up to 0.4 mm in thickness consist of heavily twinned euhedral crystals, exhibiting an orange luminescence. The second cement generation corresponds to elongated single crystals of barite, up to 1.5 mm long (Fig. 4A) formed in veins restricted to *Lst* 2 and overgrew *Cal* 1. Barite is intergrown with iron-rich saddle dolomite (*Fe-Dol*), and both precipitated during the major early cementation phase in veins and interparticle pore spaces (Fig. 5A, B) throughout the whole succession. The curved crystals of *Fe-Dol* show undulatory extinction and are cloudy in thin section with a dark gray color. In the lower part of *Dst* and in *Lst* 2, *Fe-Dol* occurs in veins perpendicular to bedding (Fig. 4A). In the upper part of the *Dst* and in *Lst* 1 and 3, *Fe-Dol* cements fill skeletal fossil molds (Figs. 5A, B) and replace aragonite and high-Mg calcite shells.

Additionally other iron-rich carbonates such as magnesium-enriched siderite and magnesium-enriched ankerite occur at the base and the top of the La Vid Group, respectively. The high iron content is identified by SEM-EDX investigation, staining (dark blue color), and CL (non-luminescent) (Schneider et al. 2004b). According to the same authors, small idiomorphic pyrite crystals are associated with siderite and *Fe-Dol*, and minor amounts of pyrite have been observed in different organic matter-rich layers and in the uppermost bed of *Lst* 3 together with green chlorite surrounding ankerite crystals.

The basal layer of the *Ts* is composed predominantly of detrital quartz grains cemented by colorless to pale greenish siderite. The composition of this cement varies from bright luminescent crystals with a Mg:Fe ratio of 1:3 to dark luminescent crystals with a 1:1 ratio. Both crystal types are Ca-poor (Schneider et al. 2004b). Ankerite was found as cement in fossil molds and pore spaces at the top of *Lst* 3 below the transition to the Esla shales. These crystals, occurring in crinoidal grainstones, are colorless, clear, and idiomorphic with a rhombic shape.

Intermediate Stage

The cements belonging to this interval reveal significant macroscopic and microscopic deformation features (Fig. 4B) such as slickenside fibers, brecciation, and intercrystalline deformation. Turbid and clear saddle dolomite (*tS-Dol* and *cS-Dol*), in addition to quartz and a second calcite cement phase (*Cal* 2), characterize this intermediate phase.

tS-Dol occurs only in veins of the *Ts* and the *Dst*. Many of these veins are irregularly shaped, oriented perpendicular to bedding, and crosscutting bedding-parallel stylolites. Veins in the lower part of the *Dst* are often associated with internal faults and folds, where this cement forms slickenside fibers on the walls of fault planes. The crystal size varies from 0.1 to 1 mm, it exhibits undulatory extinction, and crystal faces are typically curved (Fig. 5C). *tS-Dol* shows a faint blue color after staining, and dull red luminescence in contrast to the brighter colors of the host rock (Fig. 5D).

cS-Dol occurs in nodular beds of the *Dst*, cementing molds and fractures. This cement includes fragments of brecciated host rock (Fig. 5E). The clear and colorless *cS-Dol* crystals are up to 3 mm in diameter. Not all crystals show the typical saddle shape, and only a few have a faint undulatory extinction. Dolomite crystals show red luminescence with brighter colors of the rim (Fig. 5F). The remaining porosity was filled with clear quartz crystals containing only a few inclusions. This quartz cement is slightly deformed, as observed from its faint undulatory extinction. Investigated $^{87}\text{Sr}/^{86}\text{Sr}$ isotope ratios of this cement reveal values with 0.708955 before the fault zone and 0.709076 after the fault zone.

A second calcite generation (*Cal* 2) occurs in veins of *Lst* 1 to 3 and *Dst* (Fig. 4B). These veins crosscut *cS-Dol* veins, and formed at a high angle to sedimentary layering. Tension gashes opened perpendicular to layer-parallel-shortening stylolites, and were also filled by this cement. *Cal* 2 has a white color with a cloudy appearance in thin section. The

crystals are fibrous and grew perpendicular from the vein walls. The luminescence of *Cal* 2 is orange.

Late Stage

In reactivated fault zones and heavily brecciated veins of *Fe-Dol* (Fig. 4C) large amounts of a third calcite generation (*Cal* 3) were precipitated. This cement is associated with kaolinite (Raman detected) and celestite (*Cel*) as well with Fe-oxyhydroxides. An even later fourth generation of calcite cement (*Cal* 4) is related to recent karstification. *Cal* 4 crystals are clear, inclusion-poor, and nonluminescent.

Throughout the La Vid Group and other overlying carbonate formations, *Cal* 3 precipitated in veins and molds. Veins in fault zones may contain *Cal* 3 crystals up to 5 cm in diameter, where they also form slickenside fibers. In thin section, colors of *Cal* 3 vary from colorless to milky white and reddish. Crystals have a clear to cloudy appearance, depending on varying amounts of solid and fluid inclusions. In addition, these crystals have twin planes, which are either partly recrystallized or partly bent. Their luminescence colors range from orange to dull orange.

Fe-Dol and ankerite of the early stage are brecciated and calcitized with formation of Fe-rich oxyhydroxides as a by-product of dolomite dissolution, which luminesce bright orange. These alteration products also occur in the vicinity of thrust faults of *Lst* and *Dst*. Relics of *Fe-Dol* are still recognizable in highly altered parts of the rocks (Fig. 5G, H).

Cel occurs in nodular horizons of *Dst*, filling veins, skeletal molds, and pore space still open after precipitation of *Cal* 3. Moreover it precipitated in highly brecciated veins together with *Cal* 3 on fragments of earlier *Fe-Dol*. Crystals of celestite are elongated and up to 0.5 mm in length, are mostly clear, and show no preferred orientation. Small crystals of anhydrite and solid bitumen occur within celestite.

Kaolinite appears associated with *Cal* 3 in veins of the *Lst* 3 as clear, idiomorphic hexagonal crystals up to 10 μm in diameter and as bookshelves-like aggregates with a good cleavage. They show no preferred orientation of the crystallographic *c* axis. The crystals have blue-violet luminescence.

FLUID INCLUSIONS

The cements corresponding to the previously described stages contain several distinct types of aqueous and petroleum fluid inclusions (see Table 1).

Early Stage

Aqueous inclusions in *Cal* 1 are very small (diameter < 3 μm) and contain only a liquid phase (Fig. 6A). Most of the aqueous fluid inclusions in *Fe-Dol* are smaller than 2 μm in diameter and are equally distributed throughout the crystals (Fig. 6C). The presence of a small bubble is observed only in rare larger inclusions with sizes up to 5 μm . The total homogenization to the liquid phase of these inclusions occurs between 114 and 119°C (Fig. 7C). In cooling experiments nucleation of ice occurs between -44 and -46°C and is associated with the disappearance of the vapor bubble. The metastable melting of the ice occurs at -0.1°C and is marked by the sudden reappearance of the bubble. These temperatures indicate an unspecified low salinity. Gas hydrates were not detected in the fluid inclusions.

Petroleum inclusions containing a liquid and a vapor bubble are found in *Cal* 1, barite, and *Fe-Dol*. These inclusions form secondary blue-fluorescing trails crosscutting the crystals in *Cal* 1 (Fig. 6B). Although inclusions are abundant in this cement, their small size enabled only a few microthermometrical measurements. Homogenization into the liquid phase occurred in a temperature range between +32 to +102°C, with a poorly defined mode between +41 and +44°C (Fig. 7A). The bubble size

TABLE 1.—Summary of microthermometry, volume estimations and Raman spectroscopy for fluid-inclusions types in different types of cements.

Cement	Aqueous		Petroleum
	Low-salinity	High-salinity	
<i>Cal</i>	P all-liquid	—	S vol.% 10/15 T_h 41/44 (32 to 102) $n = 13$
<i>Bar</i>	—	—	P T_h (45 to 253) [#] $n = 11$ λ 452 nm
<i>Fe-Dol</i>	P mostly all-liquid T_h (114 to 119) $n = 4$	—	P vol.% 10/15 T_h 58/68 (39 to 86) $n = 19$ λ 441 nm
<i>Cs-Dol</i>	P (core) vol.% 7/9 T_h 160/170 (142 to 209) $n = 28$ T_m -1.0/-1.4 (-0.9 to -2.2) $n = 19$	P (rim) vol.% 6/9 T_h 110/120 (93 to 200) $n = 27$ T_m (ice) -27.0 to -28.8 T_m (HH) -29.3 to -29.5 $n = 4$	—
<i>Qtz</i>	P mostly all-liquid CH ₄ vapor bubble	P all-liquid @ kaolinite	—
<i>Cal3</i>	P all-liquid	—	—
<i>Cel</i>	P/S vol.% 0/100 [#] CH ₄ vapor bubble	—	—

P and **S** indicate primary and secondary inclusion origin. T_h = the temperature (°C) of homogenization into the liquid phase with the mode and range in brackets. vol.% = the volume percentage estimation of the vapor bubble. T_m = the melting temperature (°C) of ice and hydrohalite (HH). n = the corresponding number of measurements. λ = the wavelength of fluorescence. @ = accidentally trapped. # experimentally stretched.

varied from 4 to 34 vol.% with a mode between 10 and 15 vol.%. Volume percentages were estimated according to surface fractions (see the method of Bakker and Diamond 2006). Petroleum inclusions in barite have irregular shapes and are up to 20 μ m in diameter. In contrast to *Cal 1* they occur in a primary configuration. The homogenization into the liquid phase of these inclusions in barite widely varied between +45 and +253°C (Fig. 7B). Later heating runs of the same inclusions revealed higher temperatures indicating experimental stretching and decrepitation during microthermometric measurements, illustrating that these are not suitable for estimation of original fluid isochores. Fluorescence measurements of these petroleum inclusions show a wavelength of 452 nm (Fig. 8). The primary petroleum inclusions in *Fe-Dol* from *Lst 1* are in general very small (< 1 μ m). There are only few exceptions of irregular-shaped inclusions up to 10 μ m in diameter (Fig. 6D). Homogenization temperatures to the liquid phase varied from +39 to +86°C, with a mode between +58 and +68°C (see Fig. 7C), bubble sizes from 5 to 17 vol.% with a mode between 10 and 15 vol.%. Measurements of the blue fluorescence reveal a wavelength of 441 nm (Fig. 8).

The composition of the petroleum inclusions from samples of *Lst 1* including host rock and cements (*Cal 1* and *Fe-Dol*) was measured by means of gas chromatography and revealed dominantly n-alkanes with a distribution typical for mature oil. Reflectance measurements on gray

solid bitumen in the host rock of *Lst 1* gave values varying between 1.4 and 1.8% BRr (Frings, personal communication 2002), classifying the solid bitumen as epi-impsonite, which evolves only by thermal maturation of hydrocarbons already present in the rock and does not flow (Jacob 1989; Taylor et al. 1998). These values correspond to vitrinite reflectance values of 1.3 to 1.6% VRr (cf. Jacob 1989) and temperatures of 154 to 172°C, calculated after Barker and Pawlewicz (1994). Solid bitumen also occurs in *Fe-Dol*-rich veins of *Dst*, about 100 m below *Lst 1* (cf. Fig. 3). The corresponding Raman spectra reveal first-order D and G peaks of carbonaceous matter (Fig. 9A) with wave numbers of about 1370 and 1600 cm^{-1} , respectively. Second-order S2 and S3 peaks (Fig. 9B) occur at 2930 and 3200 cm^{-1} , respectively. According to Spötl et al. (1998) such spectra correspond to vitrinite reflectance values of about 1.9% VRr.

Intermediate Stage

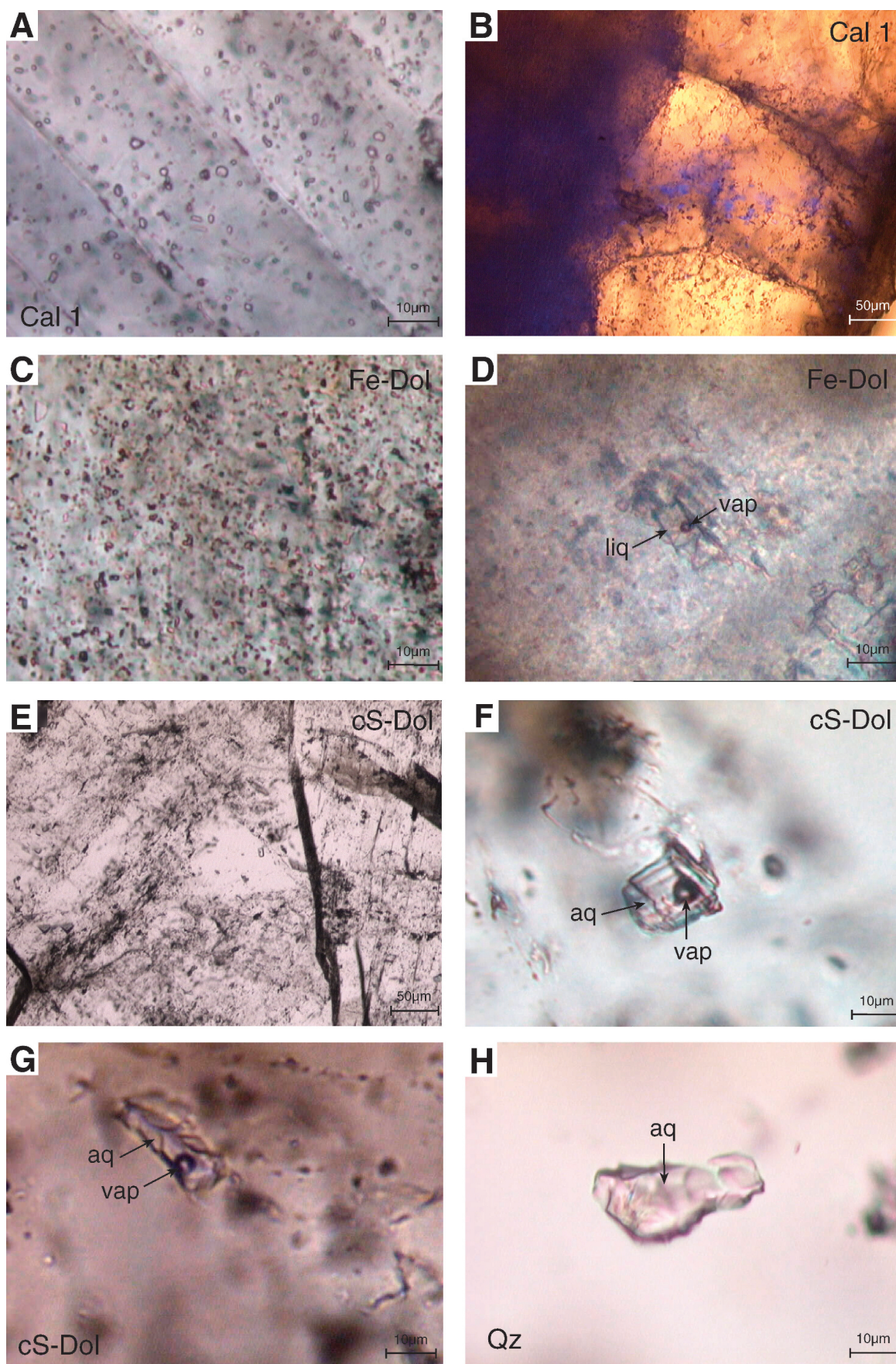
Among the cements of this stage only *cS-Dol* and *Qz* contain identifiable aqueous fluid inclusions. Two-phase inclusions (liquid + vapor) occur in growth zones in *cS-Dol* (Fig. 6E) of the crystals, which is typical for a primary configuration. The shape of the inclusions varies from elongated, equidimensional (Fig. 6F) to rectangular with sizes ranging from below 2 μ m to 15 μ m in diameter. In the vapor phase of some inclusions traces of methane were detected in Raman spectra.

The melting temperatures exhibit two different kinds of aqueous inclusions in *cS-Dol*: low-salinity and high-salinity. The low-salinity inclusions (Fig. 6F) occur in the core of the crystals close to the host rock whereas high-salinity inclusions (Fig. 6G) are located in the rims. Both contain similar amounts of vapor bubble fraction. Nucleation temperatures during freezing experiments of the low-salinity inclusions vary between -42 and -44°C and the vapor bubble remains present. Final melting temperatures of ice range between -0.9 and -2.2°C with a mode between -1 and -1.4°C (Fig. 10). Gas hydrates were not detected. Nucleation temperatures of the high-salinity inclusions vary between -69 and -79°C.

Detailed analyses of the phase changes in these inclusions during heating and freezing experiments were obtained from the combination of Raman spectroscopy and microthermometry (see also Bakker 2004). After fast cooling (40°C/min) to -180°C, only ice and a high-salinity aqueous liquid solution were detected. During specific cycling several types of salt hydrates were cultivated inside the inclusions. The Raman spectrum (Fig. 11A) reveals a combination of ice in addition to a complex hydrate spectrum consisting of multiple components. It cannot be assigned to one specific type of salt hydrate, but contains possibly elements of magnesium-chloride hydrate and hydrohalite (cf. Bakker 2004). In a different heating-freezing cycle inclusion spectra of only ice and hydrohalite were obtained (Fig. 11B) in the metastable absence of the other salt hydrate. The final melting temperatures of ice and hydrohalite were measured in several inclusions by recording Raman spectra during stepwise heating (Table 1). Hydrohalite melted between -29 and -30°C, a cotectic melting, and ice finally melted between -27 and -28°C. The melting temperatures of the possible MgCl₂ hydrates were approximately estimated at -42°C. This low temperature indicates the presence of unspecified dissolved cations, inasmuch as it is below the eutectic temperature of the ternary fluid system H₂O-NaCl-MgCl₂ (i.e. -35°C).

The homogenization into the liquid phase of the low-salinity inclusions in *cS-Dol* occurs in the range of 142 to 209°C with a mode between 160 and 170°C (Fig. 12). High-salinity inclusions homogenize also into the liquid phase, over a much broader range from 73 to 200°C with a mode at lower temperatures (110–120°C) as well as at higher temperatures (190–200°C).

Quartz contains only a small number of inclusions with irregular shapes and sizes up to 10 μ m in diameter (Fig. 6H). They have a broad compositional variety. Low-salinity fluids with a methane bubble were identified in some inclusions (Fig. 13A). Furthermore, highly saline, all-



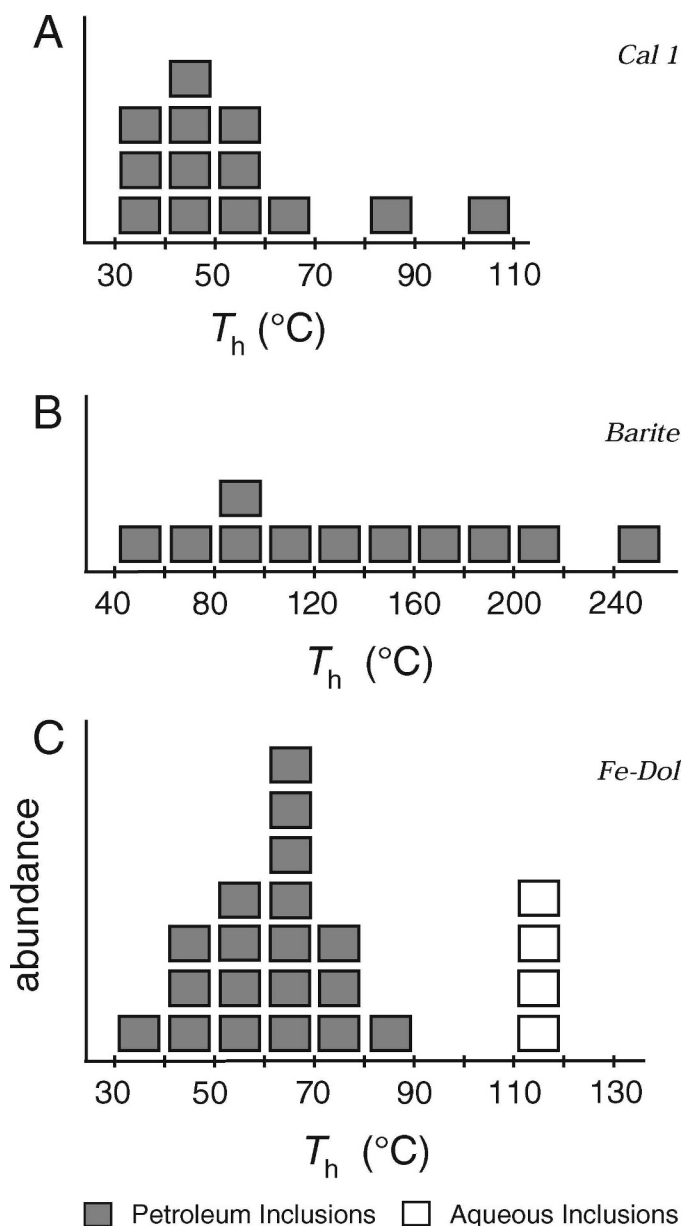


FIG. 7.—Histogram of homogenization temperatures (T_h) of the petroleum and aqueous inclusions in A) *Cal 1*, B) barite, and C) *Fe-Dol*.

liquid fluid inclusions (Fig. 6H) were identified by Raman spectroscopy (Fig. 13B, cf. fig. 7 in Bakker 2004). Some of the high-salinity inclusions have small accidentally trapped kaolinite crystals (Fig. 13C, Raman detected), which differs from the previously mentioned massive kaolinite that occurred in the late stage (see Cement Petrography). Heating and freezing experiments to specify the salinity of individual inclusions were not successful.

FIG. 6.—Microphotograph of fluid inclusions: A) all-liquid aqueous fluid inclusions in *Cal 1*; B) trail with fluorescing petroleum inclusions crosscutting *Cal 1*-crystals; C) tiny all-liquid aqueous fluid inclusions in *Fe-Dol*; D) irregular-shaped two-phase petroleum inclusion in *Fe-Dol*; E) zonation in *cS-Dol* with areas of lower and higher inclusion density; F) large low-salinity fluid inclusion in *cS-Dol*; G) irregular-shaped high-salinity fluid inclusions in *cS-Dol*; H) all-liquid inclusion in *Qz*. liq = liquid phase (petroleum), vap = vapor bubble, aq = aqueous liquid solution.

Late Stage

A zonation in the crystals of *Cal 3* is marked by the distribution of fluid inclusions (Fig. 14A). High-density zones of fluid inclusions alternate with nearly inclusion-free zones. The inclusions have an irregular shape (Fig. 14B), but the walls are defined by the crystallography of the host. The inclusions contain only a low-salinity, liquid aqueous phase. Locally, small bubbles (< 1 vol.%) are present in these inclusions.

Fluid inclusions in celestite occur in primary growth zones (Fig. 14C) or in secondary healed fractures (Fig. 14D). The shape of the inclusions varies from regular, perfectly negative crystals to highly irregular. They have a broad variety of contents: all-liquid, aqueous liquid plus a CH_4 -rich vapor bubble. The volume fraction of the liquid varies between 0 and 100% (Fig. 14C). Consequently total-homogenization temperatures occur in a large range up to 211 °C similar to the fluid inclusions in barite, again illustrating experimental stretching and decrepitation. Nucleation temperatures during freezing experiments in aqueous liquid-rich inclusions are around -34 °C. Final melting temperatures occur at about -0.1 °C, indicating the presence of nearly pure water.

MODELING OF PETROLEUM AND SALINITY

The composition of individual petroleum fluid inclusions was modeled similarly to the PIT model (Thiery et al. 2000). The composition of different types of oil can be summarized in a two-component mathematical equation: including an a and a b value (see Montel 1993). These values do not vary independently, and a natural trend in oil compositions reveals several unique values for a and b (see Thiery et al. 2000). Different types of oil, which are trapped in fluid inclusions, have a homogenization behavior specific for each type. In other words, for each a and b value an immiscibility field can be calculated within a P-T diagram illustrating all possible homogenization conditions. For example, homogenization into the liquid phase at 100 °C can be applied to only a limited range of compositions, i.e., a and b values. The intersection of the previously described trend of natural oils and this limited range indicates the composition of the oil in the fluid inclusion with the selected homogenization temperature. The major assumption is that the trapped oil in the inclusions is part of this natural trend. For *Cal 1* a and b values range from 0.84 to 0.88 and 0.54 to 0.65, respectively, with a mean of 0.86 and 0.60. This composition is similar to known compositions of light and critical oils from North America (Thiery et al. 2000). The oil in the *Fe-Dol* reveals different a and b values ranging from 0.88 to 0.90 and 0.39 to 0.57, respectively, with a mean of 0.89 and 0.48. The modeled compositions of the latter oils display a range similar to the light and heavy oils from North America.

The aqueous fluids in the inclusions of *Cal 1* and *Fe-Dol* can be interpreted as marine to meteoric water. Similar fluids are found in the internal growth zones of the *cS-Dol*. A sudden change to high-salinity fluids occurs in external growth zones of the *cS-Dol* crystals. The salinity of those inclusions (see Table 1) can be modeled in ternary H_2O - NaCl - MgCl_2 or H_2O - NaCl - CaCl_2 systems. Although Raman analyses did not conclusively indicate the presence of either MgCl_2 or CaCl_2 , NaCl has been positively identified in this aqueous solution as hydrohalite at low temperatures. The second type of salt (MgCl_2 or CaCl_2) has been selected to model salinities in a ternary system according to the microthermometric observations (use of equivalent mass %). True eutectic temperatures have not been detected. The salinity has been calculated using the model of Dubois and Marignac (1997) and the computer program *AqSo3*

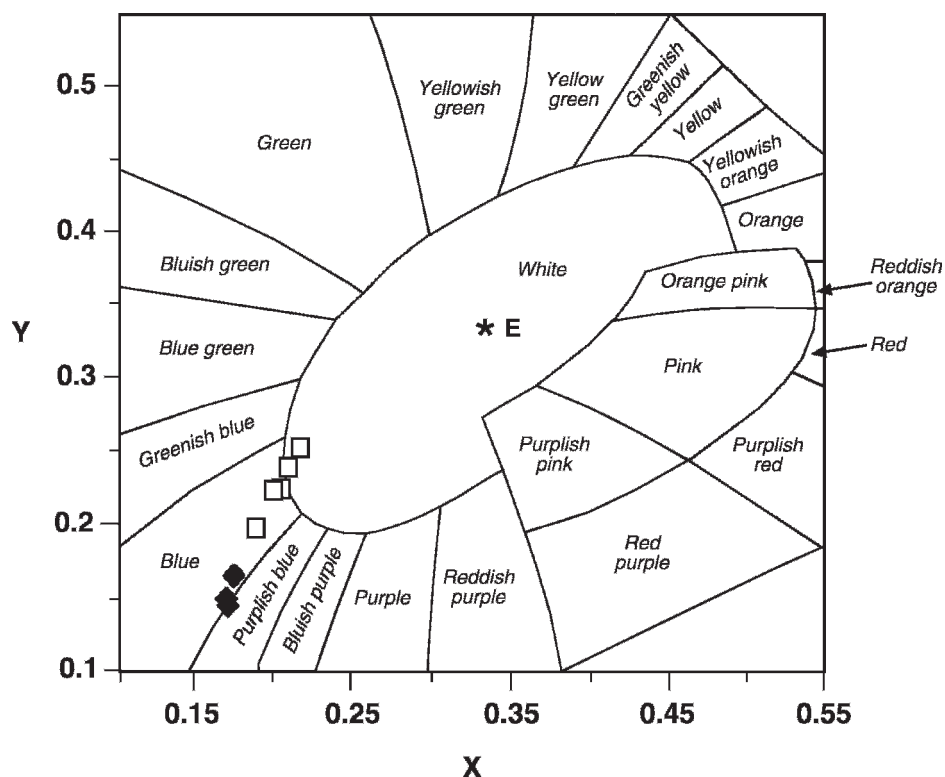


FIG. 8.—Diagram with the chromaticity coordinates (CIE 1931) for the oil inclusions of *Fe-Dol* (squares) and barite (diamonds). The individual fields represent approximate color regions. E is the achromatic point ($x = \frac{1}{3}$, $y = \frac{1}{3}$)

from Bakker (2003). Salinities of 8.9 to 9.3 mass % NaCl and 15.1 to 15.4 eq.mass % MgCl_2 have been calculated. Alternatively, similar calculations in the ternary H_2O –NaCl– CaCl_2 system result in 7.0 to 7.4 mass% NaCl and 17.9 to 18.2 eq.mass % CaCl_2 (Naden 1996, and computer program *AqSo2*, Bakker 2003). Both calculations illustrate that NaCl is not the major constituent of salts in the aqueous solution.

INTERPRETATION

The studied cements precipitated after the early diagenetic dolomitization that affected the host-rock carbonates and formed massive replacement dolomite within the lower part of the succession (see Fig. 3). The cement precipitation took place during burial in a relatively undisturbed rock succession. Therefore, the studied section is ideally suited to determine quantitatively and qualitatively the effect of temperature and pressure on fluid chemistry and diagenetic processes in the specific lithology of the La Vid Group. The previously described

stages of cement precipitation in veins and skeletal molds with corresponding parental fluids can be related to distinct events of the Variscan and Alpidic orogenies.

Early Stage: Pre-Variscan Basin Stage

The three early-stage cements in the La Vid Group of the Cantabrian Zone reveal an evolutionary trend during the pre-Variscan basin stage up to the Variscan orogenesis. *Cal 1* as the first cement indicates formation conditions below 50°C (low P–T conditions) based on the presence of all-liquid primary aqueous inclusions in the crystals (cf. Goldstein and Reynolds 1994). Normally, the relative low strength of calcite does not allow the survival of these inclusions during a prograde burial heating. However, this is highly dependent on the size, shape, and distribution of inclusions (Leroy 1979). Especially small inclusions may survive high overpressures.

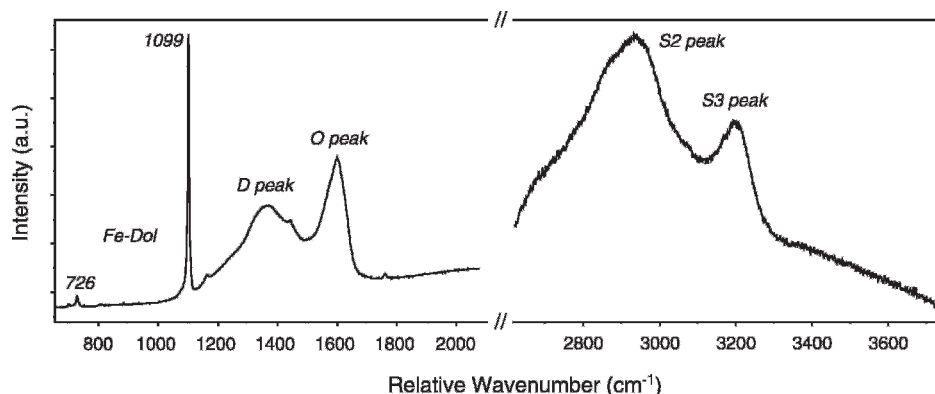


FIG. 9.—Representative first-order (D peak and O peak) and second-order Raman spectra (S2 peak and S3 peak) of the bituminite inclusions in *Fe-Dol* from the *DST*.

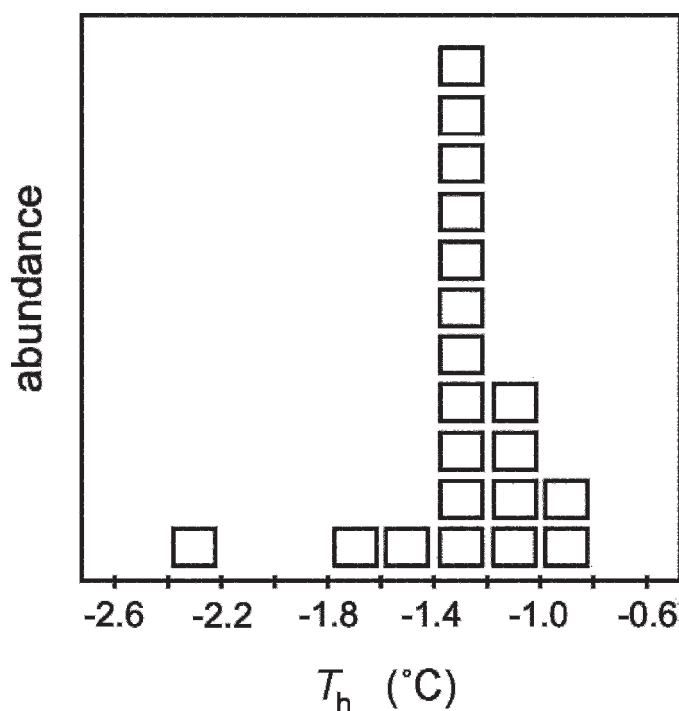


FIG. 10.—Histogram of melting temperatures (T_m) of the low-salinity inclusions in *cS-Dol*.

Petroleum was introduced in a later burial stage, during growth of barite, and was trapped as secondary inclusions in *Cal* and primary inclusions in barite. A coexisting aqueous fluid was also preserved in primary inclusions in barite. Consequently, both petroleum inclusions in *Cal* and barite should reveal similar homogenization temperatures. However, a definitive estimation of homogenization and trapping conditions in barite could not be established due to the weakness of the mineral that caused post-entrapment stretching and decrepitation, partly induced during preparation and microthermometry of the samples (notice the wide spread in T_h in Fig. 7B).

In the final stage of basin evolution *Fe-Dol* precipitated from a low-salinity aqueous solution in the presence of another petroleum fluid that is distinctly different from the previously described petroleum in barite. Only part of the aqueous fluid inclusion in *Fe-Dol* reveal the presence of a small bubble. Aqueous fluid inclusions with high filling degrees, i.e., high densities and small volume fractions of stable vapor bubbles, may remain in a metastable liquid state at room temperatures because of nucleation difficulties of the vapor bubble (see also Goldstein and Reinholds 1994). Therefore, the measured homogenization temperatures are regarded to represent stable homogenization conditions of most fluid inclusions.

The salinity of these aqueous inclusions corresponds to meteoric or marine water. These petroleum and aqueous inclusions probably belong to one fluid inclusion assemblage, as deduced from their distribution in single grains. Both occur in a similar configuration, which can be marked as primary inclusions, and can, therefore, be formed only (almost) simultaneously during growth of the crystal. Chemically, the coexistence of both fluids in *Fe-Dol* could not be proven. Consequently, trapping conditions can be modeled according to either an assumed thermal gradient (*PT2* in Fig. 15) or the intersection of isochores at total homogenization of the aqueous solution (*PT1* in Fig. 15). The isochores of the aqueous fluid inclusions are based on a pure H_2O composition, which simplifies the fluid modeling. If petroleum and aqueous inclusions belong to the same assemblage, hydrocarbons (especially CH_4) must be

dissolved in the aqueous solution in those inclusions in the absence of vapor bubbles. The detection limit of Raman, however, did not allow estimation of these small amounts, and it has no significant effect on the slope of the isochores. Although there is no direct proof for the magnitude of the paleo-geothermal gradient in these rocks, an average gradient of $35^\circ/km$ is assumed for this part of the upper crust (Brime et al. 2001) during basin subsidence. Its intersection with isochores of aqueous inclusions (*PT2* in Fig. 15) corresponds to a burial and formation pressure of *Fe-Dol* of about 38.5 to 40.5 MPa, which indicates a depth of 3850 to 4050 m and a corresponding burial temperature of approximately 130 to 140°C if a hydrostatic geothermal gradient is assumed for the pore fluid. The intersection of petroleum inclusion isochores and the measured homogenization temperatures of aqueous fluid inclusions (see also Thiéry et al. 2000) reveal similar trapping conditions (*PT1* in Fig. 15). The spread of calculated petroleum densities is reflected in the spread in trapping conditions, 37 ± 10 MPa. The depth of about 4000 m calculated above would, however, be greater than the accumulated stratigraphic thickness from Lower Devonian to upper Carboniferous, which is up to 3100 m thick in this part of the Somiedo-Correcillas Unit. This might indicate a thickening of these units towards the study area. An alternative explanation would be fluid overpressures during trapping, which are common in active petroleum systems (Law and Spencer 1998; Broichhausen et al. 2005). Under such conditions high pressures can be expected at shallower depths. However, such conditions would require the assumption of higher heat flows and geothermal gradients for the upper crust than assumed above.

The calculated P-T conditions obtained from the petroleum and aqueous inclusions in *Fe-Dol* illustrate therefore the preservation of prograde fluid properties during burial in the basin stage, up to the time when peak diagenetic conditions were reached. Also the difference in homogenization temperature of petroleum inclusions in *Cal 1* (41–44°C) and *Fe-Dol* (58–68°C) indicated the preservation of a prograde fluid evolution.

Thermodynamic modeling of the oil indicates that the oil in *Cal 1* is lighter than the oil in *Fe-Dol*. The higher wavelength of fluorescence of the oil in barite (452 nm) that occurs in a slightly higher stratigraphic position than *Fe-Dol* (441 nm) coincides with a shift to a slightly lower degree of maturation (Burruss 1981; Hagemann and Hollerbach 1985; McLimans 1991). From the wavelength an API gravity of about 45° (see Bodnar 1990) is estimated. The high maturity is also revealed by gas chromatography, with a dominance of the n-alkanes corresponding to the presence of mature oil in *Fe-Dol* and the surrounding host rocks. The occurrence of epi-impsonite in these host rocks points to an even higher degree of maturation (see below). The origin of the oil in *Cal 1* must have been a more mature source rock, or the entrapment of the oil must have occurred at a later stage at higher P-T conditions, when a more mature (lighter) oil was trapped in secondary inclusions. This explanation must be excluded, inasmuch as the homogenization temperatures in *Fe-Dol* are distinctively higher than in *Cal 1*. We assume that the main part of maturation was pre-orogenic, but this cannot be deduced directly from the data presented here.

The origin of the low-salinity aqueous fluid and the petroleum can be attributed to formations stratigraphically below the La Vid Group (cf. Schneider et al. 2004a). The Silurian graptolite-bearing Formigoso shales contain abundant organic matter from which oil could have been generated when the temperatures reached the oil window. Additionally, clay-mineral diagenesis in these shales could have released Mg (e.g., Foscolos 1990) necessary for the formation of *Fe-Dol*. During upward migration these fluids absorbed ferric iron from the hematite-bearing Silurian San Pedro Fm. because of its reducing character and precipitated different Fe minerals in the overlying La Vid Group (Schneider et al. 2004a).

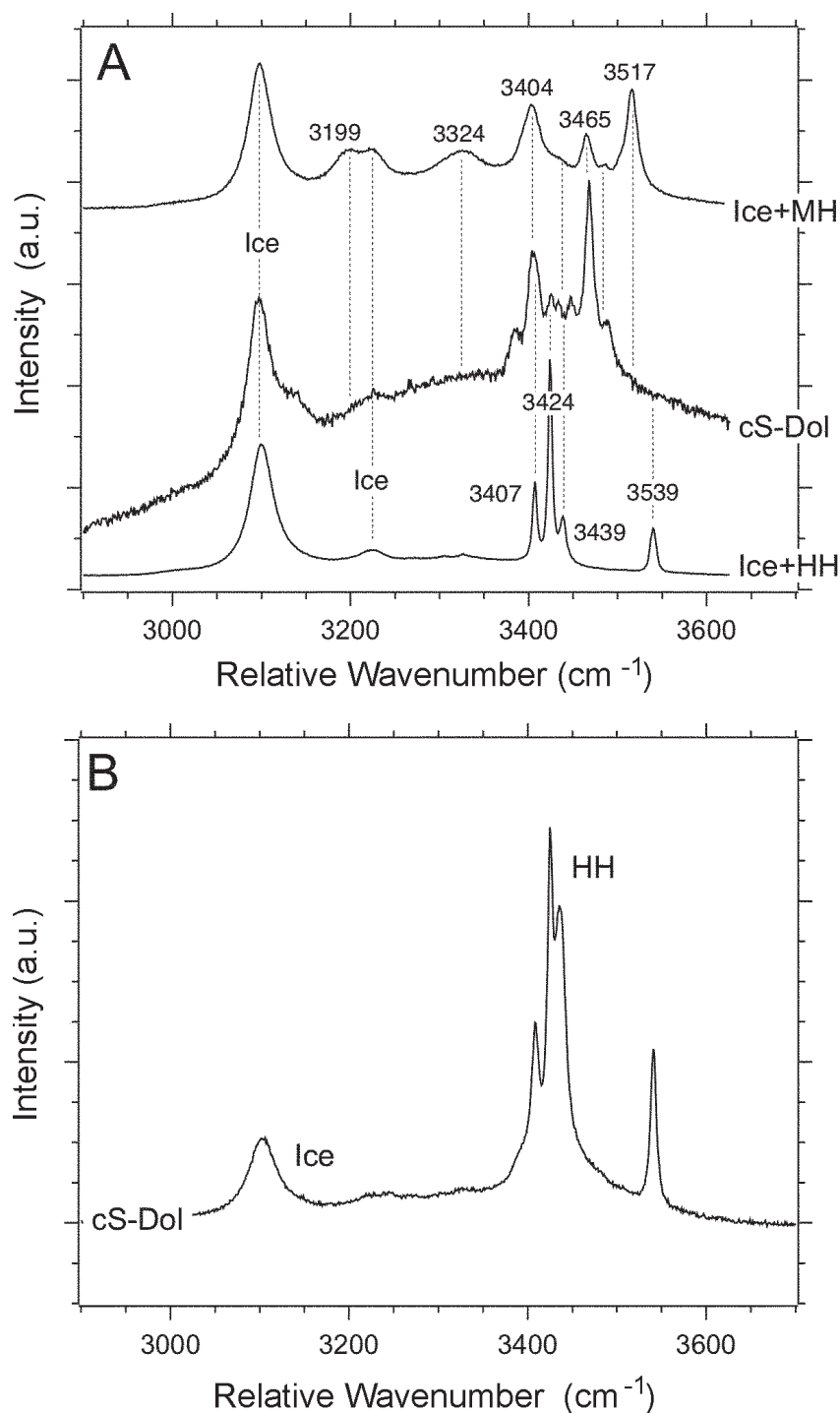


FIG. 11.—**A**) Comparison of the identified Raman spectra of a complex hydrate in the high-salinity inclusions of *cS-Dol* with the standard spectra for magnesium-chloride hydrate (Ice + MH) and hydrohalite (Ice + HH) from Bakker (2004). **B**) Raman spectrum of the metastable mixture of hydrohalite (HH) and ice in a high-salinity inclusion of *cS-Dol*.

Intermediate Stage: Syn-Variscan to Late-Variscan Stage

The intermediate stage corresponds to a stage of tectonic activity (brecciation and fracturing, see also Figure 4B) and is therefore attributed to the Variscan orogeny. This is also the time of highest temperatures. The already mentioned occurrence of epi-impsonite in the host rock points to a high degree of maturation, due to its *in situ* formation by cracking of oil at high temperatures (cf. Jacob 1989). Similar solid bitumen also occurs as inclusions in *Fe-Dol* from veins in the *Dst*. Calculated vitrinite reflectance values of the epi-impsonite reveal

temperatures between 154 and 172°C according to the equation of Barker and Pawlewicz (1994). Possibly these maximum temperatures were reached in the La Vid Group already at the end of the basin stage of the Paleozoic sediments (Brime 1985; see also Keller and Krumm 1993, Raven and van der Pluijm 1986, Brime et al. 2001), but more likely thereafter, during orogenesis (nappe stacking and orocline formation): a thermal peak occurred in Late Stephanian and especially Early Permian time, when crustal thinning, intense volcanism, and sparse plutonism took place in a predominantly extensional setting of the outer part of the Cantabrian orocline (Gutiérrez-Alonso et al. 2004). Aller (1986) invoked

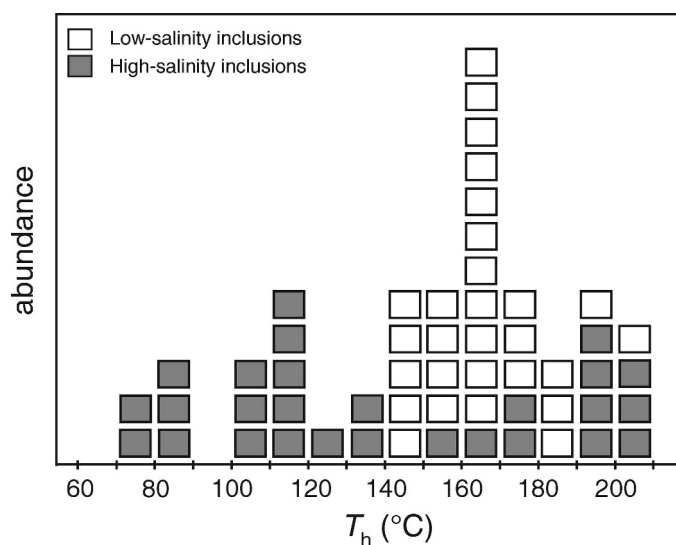


FIG. 12.—Histogram of homogenization temperatures (T_h) of low-salinity and high-salinity aqueous inclusions in *cS-Dol*.

a “high geothermal gradient at the transition from Carboniferous to Permian” to explain metamorphism and cleavage in the Central Coal Basin farther to the north (inner part of the orocline). Frings et al. (2004) investigated paleotemperature anomalies of the Stephanian Ciñera–Matallana basin to the south and proposed a geothermal gradient approaching 85°C/km. This assumed high gradient is related to Early Permian magmatic activity localized within the Stephanian coal-basin successions and cannot be extrapolated to areas outside these local extensional basins. Gasparrini et al. (2006a) calculated maximum trapping temperatures of around 150°C during latest Carboniferous to Early Permian massive dolomitization of lower Carboniferous rocks. These data relate to outcrops in the Bodon tectonic unit to the north, situated below the Somiedo–Correcillas unit where the La Vid section is

positioned. Lapponi et al. (2004) and Lapponi et al. (2005) calculated trapping temperatures around 120°C for the latest Carboniferous to Early Permian epigenetic dolomites in the Cambrian succession situated at the base of the Somiedo–Correcillas thrust.

Most of the microthermometric data for this stage is obtained from *cS-Dol* that precipitated only in the *Dst* of the La Vid Group. The limited occurrence of *cS-Dol* may reflect a locally decreased porosity and permeability of the rock due to further burial during nappe emplacement. A change in fluid properties during formation of *cS-Dol* is recorded, however, by its microthermometric zonation: cores contain nearly pure water whereas rims contain a high-salinity fluid. The assemblage of low-salinity fluid inclusions in the core has a normal distribution in the T_h -frequency diagram (Fig. 12) around 160 to 170°C, with no indications of possible re-equilibration patterns. The high-salinity inclusions assemblage in the dolomite rim illustrates a broad range of T_h values (Fig. 12), which may have resulted from re-equilibration processes in a later stage of diagenesis in the basin. The initial growth of the dolomite occurred with a nearly pure-water pore fluid around 160 to 170°C. This corresponds to the maximum temperatures for burial of the rocks based on the epimponite reflectance data as outlined above. The trapped fluid inclusions remained intact during further diagenesis. The spread of T_h values only in the rim is, therefore, more likely to have resulted from variable trapping condition than from re-equilibration processes. A certain amount of post-entrapment re-equilibration during further Variscan and Alpine deformation cannot be excluded, but it should have affected both types of fluid inclusions assemblages.

Some difficulties may arise from the interpretation of the source of the high-salinity fluid. Evaporites or any relics are not known in the Cantabrian Zone. Although locally restricted lagoons existed, as can be deduced from the facies of the Santa Lucia and Portilla fms., which occur stratigraphically above the La Vid Group, the conditions were not hypersaline. However, this high-salinity brine has been identified over a wide stratigraphic range within the Cantabrian Zone and has a regional occurrence as well: (1) a high-salinity fluid was identified by Gasparrini et al. (2006b) as being responsible for the epigenetic late Carboniferous to Early Permian dolomitization in the Carboniferous limestones of the

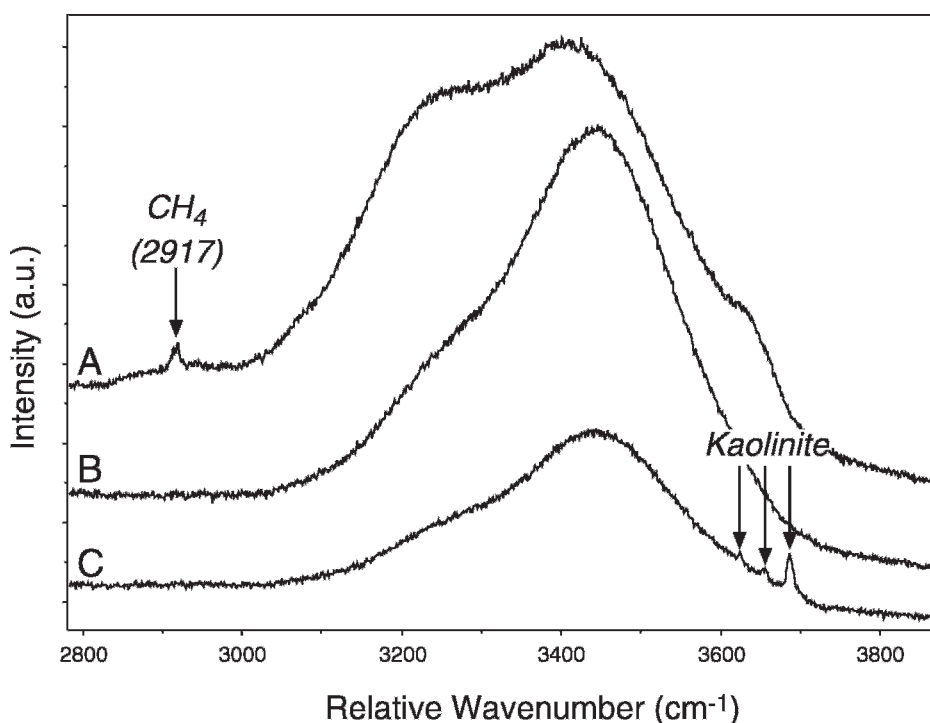


FIG. 13.—Raman spectra of fluid inclusions in quartz: A) low-salinity two-phase fluid inclusion with methane and other hydrocarbons in the vapor bubble; B) high-salinity all-liquid fluid inclusion; C) high-salinity inclusion with accidentally trapped kaolinite crystal.

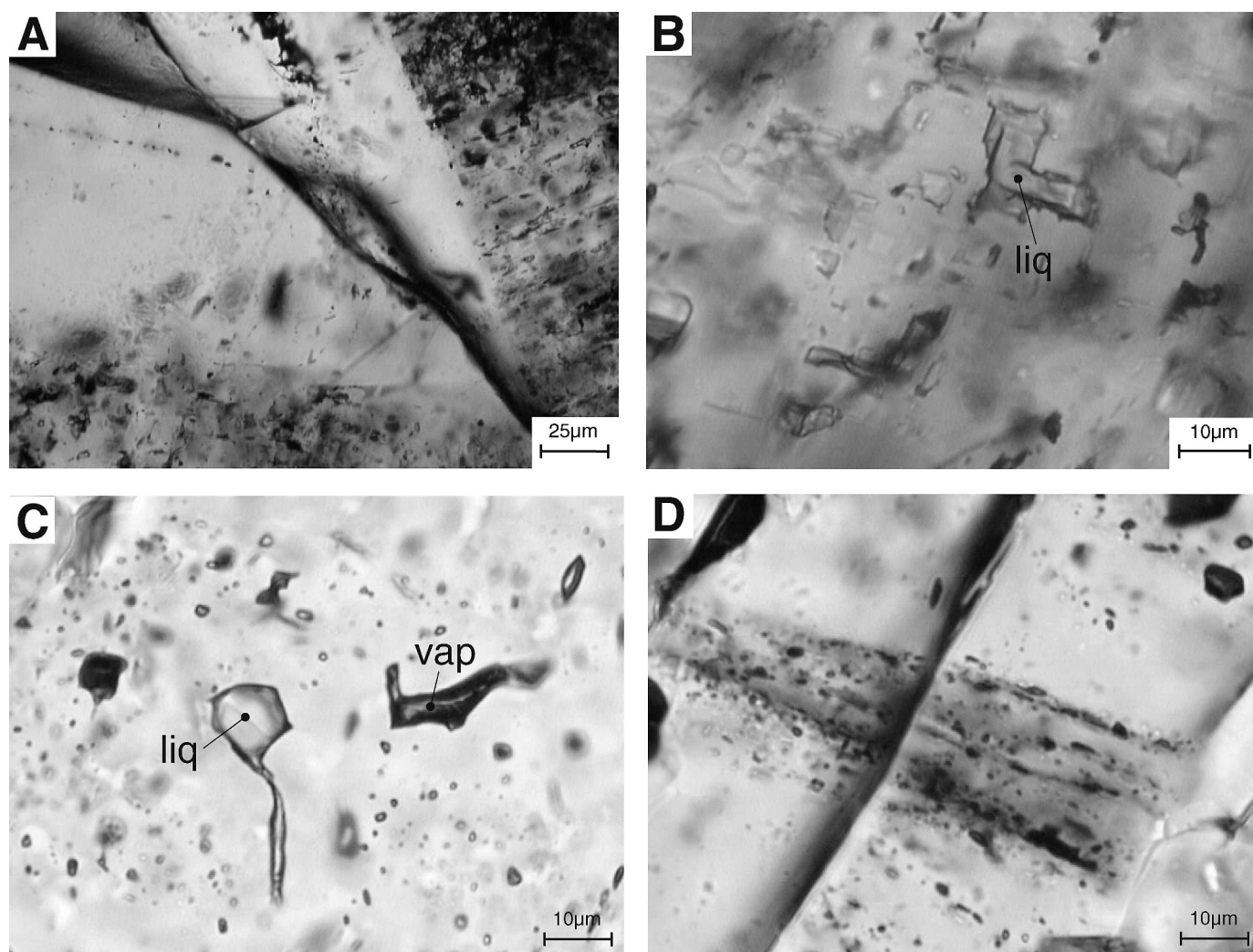


FIG. 14.—Zonation in *Cal 3* as defined by **A**) inclusion-free crystallization and **B**) irregular-shaped all-liquid fluid inclusions. **C**) Irregular-shaped all-liquid and all-vapor aqueous fluid inclusions in *Cel* and **D**) trails with secondary inclusions crosscutting crystal borders.

Barcaliente and Valdeteja fms. of the Bodon Unit north of the La Vid outcrops investigated; (2) Lapponi et al. (2004) and Lapponi et al. (2005) analyzed the same type of fluid dolomitizing the Cambrian Lancara carbonates at the thrust base of the Somiedo–Correcillas Unit, in which the La Vid section is situated; (3) Ayllón et al. (2003) described high-salinity fluids in inclusions in quartz and calcite mineralizations as well as methane in inclusions in quartz within the Ciñera–Matallana coal basin (see Fig. 1) a few kilometers farther to the south. A similar fluid is found within the quartz in the section studied here (Table 1).

The $^{87}\text{Sr}/^{86}\text{Sr}$ isotope ratios of *cS-Dol* are elevated in comparison to the adjacent dolomitic host rocks (0.708801; Schneider et al. 2004a) and Devonian or Carboniferous seawater (0.70804 to 0.708359; Veizer et al. 1999), similar to the radiogenic ratios observed in dolomitic cements in nearby Carboniferous (Gasparrini 2003) and Cambrian rocks (Lapponi et al. 2004; Lapponi et al. 2005). This might be explained by either interaction with siliciclastics or the contribution of a sialic magmatic component. The $^{87}\text{Sr}/^{86}\text{Sr}$ ratios calculated for the Peña Prieta stock and corrected to 270–275 Ma range between 0.7045 and 0.7069 (Gallástegui et al. 1990), in agreement with the intermediate to basic nature of the intrusions. These magmatic rocks show therefore a lower ratio than the host rock and can be excluded as source of the radiogenic strontium (see also Gasparrini 2003, Lapponi et al. 2004, Lapponi et al. 2005).

Precambrian to Middle Devonian shales, cropping out all over the Cantabrian Zone, contain highly radiogenic $^{87}\text{Sr}/^{86}\text{Sr}$ ratios (corrected to 270–275 Ma) between 0.7090 and 0.7731 (Nägler 1990). These are probably the source for the increased ratios within the La Vid Group, indicating a contact of the fluids, later precipitating *cS-Dol*, with these clastics. The origin of this fluid is unclear. Possibly a more or less isolated low-salinity fluid slowly evolved to a highly saline aqueous solution, due to water–rock interaction (contact with clastics) during diagenesis. The widespread occurrence of a high-salinity fluid (Gasparrini 2003; Gasparrini et al. 2006a; Gasparrini et al. 2006b; Ayllón et al. 2003; Lapponi et al. 2004; Lapponi et al. 2005), indicating relatively uniform hydrochemical conditions, makes another scenario more likely: mixing of an internally generated low-salinity fluid with a highly saline external one, causing the outer high-salinity rim of *cS-Dol*. Precipitation of *cS-Dol* stopped soon thereafter. There is no massive dolomitization in the Devonian, in contrast to the Carboniferous successions in the north. This indicates that a more open fluid system was present for only a limited period of time and to a minor degree able to enter the Devonian succession, due to their differing porosity and permeability evolution: fluid flow was focused in the higher-permeability areas, for instance in the unconsolidated sediments of the coal basins (Ayllón et al. 2003), along large fracture zones as the Somiedo–Correcillas thrust (Lapponi et al.

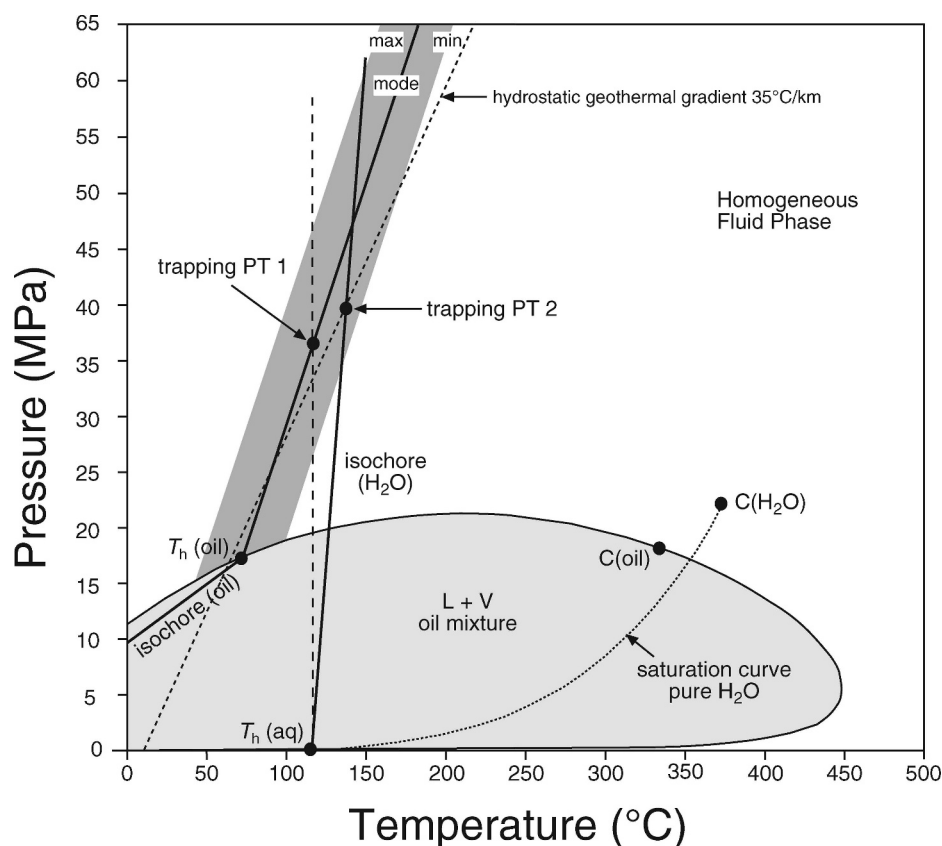


FIG. 15.—Temperature–pressure diagram illustrating formation conditions of petroleum and aqueous inclusions of *Fe-Dol* during early stage (basin stage). The gray-shaded area illustrates immiscibility P–T conditions of a light oil condensate (L + V), of composition similar to that of the oil analyzed in *Fe-Dol*, with its critical point at C (oil). This envelope is intersected by the isochore for the oil trapped in *Fe-Dol* at the respective homogenization temperatures of these inclusions (dark shade area between mode, min and max). Point PT 1 indicated trapping temperature–pressure conditions at T_h (114°C) of coexisting aqueous inclusions (35.9 MPa). Alternatively, PT 2 represent trapping conditions of only the aqueous inclusions according to the intersection of their isochores and a hydrostatic geothermal gradient of 35°/km (dotted line) revealing approximately 139°C and 39 MPa. The saturation curve and critical point of pure H₂O are illustrated for comparison.

2004; Lapponi et al. 2005) and in the dolomites near the Asturian coal basin in the north, which enhanced their porosity during the dolomitization process (Gasparrini 2003; Gasparrini et al. 2006a, Gasparrini et al. 2006b). The La Vid area had a differing diagenetic evolution from the very beginning, and had a connection with the other regions mentioned only for a short period. This period corresponds to the orocline formation, when extension and crustal thinning caused intense fluid circulation. This only brief hydraulic connection to the surrounding area is further corroborated by the fact that fibrous calcite crystals (*Cal 2*) following *cS-Dol* and crosscutting it are petrographically and fabric-wise totally different from highly saline, slightly radiogenic blocky and xenotopic calcites, occurring in the epigenetically dolomitized areas after the last generation of dolomite (Dol B, Gasparrini 2003; Gasparrini et al. 2006a; Gasparrini et al. 2006b). These calcites were formed due to a decrease in temperature of the fluids and/or an increase in the Ca/Mg ratio.

Late Stage: Post-Variscan Stage

The last fluid event is related to a second tectonic phase, which must have occurred after the Variscan orogeny and included the reactivation of faults, brecciation, and deformation of the previously precipitated cements.

The trapped low-salinity fluids in *Cal 3* and *Cel* are distinctively different from the fluids in the Variscan stage. Similarly to *Cal 1* in the early stage, *Cal 3* precipitated at relatively shallow conditions in a nearly pure aqueous solution. This low-temperature environment is also indicated by the occurrence of kaolinite (cf. Srodon 1999), which precipitated in large amounts. There is no relation of this generation of kaolinite 2 to the accidentally trapped small single crystals of kaolinite 1 in inclusions in quartz of the intermediate stage. Moreover, kaolinite 1

occurs within high-salinity inclusions, whereas the later kaolinite 2 generation is related to the low-salinity fluid of *Cal 3*.

Recrystallization of the *Fe-Dol* resulted in the formation of a mixture of Fe-oxyhydroxides and calcite, apparent in brownish patches in the rocks. The restricted occurrence of celestite within the *Dst* points to sulfate and Sr remobilization within the lower part of the La Vid Group (see also Hanor 2000). Inclusions in celestite show a broad variety in composition and density. Locally, small anhydrite crystals (most probably relics) were trapped as solid inclusions in the celestite. The presence of the sulfate nodules in the *Dst*, presumably originally containing anhydrite as source for Sr and sulfate, reflects a short migration path and the local character of these cements. Inclusions in celestite show a broad variety in composition and density. Solid bitumen and oil inclusions in celestite were probably recycled from brittle deformed veins of *Fe-Dol*, which were heavily brecciated by the renewed tectonic activity. Most inclusions contain a single phase, consisting of an aqueous solution. The two-phase inclusions unraveled the low-salinity character of the fluid corresponding to a composition between meteoric water and seawater. The highly variable phase ratios and the presence of all-liquid inclusions illustrate shallow formation conditions in the vadose zone.

Cal 3, Fe-oxyhydroxides, as well as kaolinite were observed throughout the La Vid Group and also in the overlying Santa Lucia Fm. Especially in the vicinity of faults, where a high fluid-flow can be expected, these cements occur in high quantities. This last cementation phase occurs in various locations in the Cantabrian Zone. Gasparrini (2003) describes a fluid with similar characteristics that precipitated calcite as the last phase in the paragenetic succession. This cement occurs in the Carboniferous carbonates and postdates the epigenetic dolomitization that is assumed to be Permian in age. A similar calcite cement was also observed by Immenhauser et al. (2002) in Carboniferous carbonates in the northern part of the Cantabrian Zone.

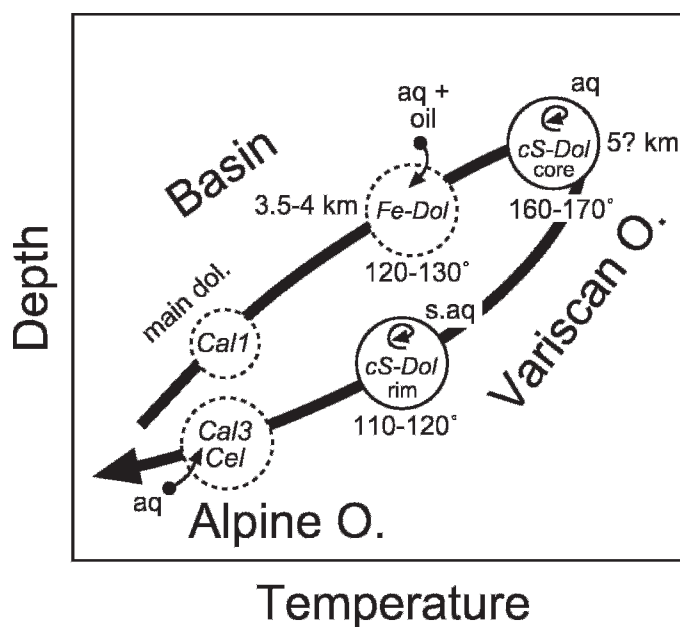


FIG. 16.—Schematic temperature–depth diagram illustrating the evolution of the La Vid Group after the main dolomitization (main dol.) during the basin stage, the Variscan stage and the Alpine stage. Open circles indicate an open system where external fluids can flow through the rock (aq = aqueous fluids and oil = petroleum fluids). Closed circles illustrate relatively closed fluid system in the Variscan stage, where the salinity increased drastically (s.aq = highly saline fluids).

CONCLUSIONS

Microthermometry and detailed geochemistry of cements can help in the recognition of fluid sources, and closed or open rock systems, further characterizing fluid–rock interaction processes. The latter provide important arguments for reconstruction of basin evolution after sedimentation. The lower Devonian La Vid Group of the Paleozoic Cantabrian Basin (northern Spain) reveals the presence of several types of cements that have evolved after a first early diagenetic dolomitization event and which reflects the interaction of local and regional fluids within these carbonate rocks and their relation to the structural evolution of the orogen.

Three types of cements evolved during a pre-Variscan basin to Variscan stage: calcite, barite, and Fe-rich dolomite, which precipitated in pore spaces, veins, and fossil molds under prograde burial conditions (Fig. 16). Low-salinity aqueous fluids and petroleum fluids with different maturities migrated through the system and were entrapped at various P–T conditions: first calcite (< 50°C, low pressure), later barite, followed by Fe-rich dolomite (130–140°C and 34.5–36.5 MPa).

During the Variscan collision and the subsequent formation of the Cantabrian orocline, turbid saddle dolomite, clear saddle dolomite, and quartz precipitated in tectonically affected veins and host rock at maximum diagenetic conditions (Fig. 16). In this stage the fluid properties changed as the system became more isolated at first and the porosity and permeability decreased drastically. A low-salinity aqueous fluid marked the beginning of this stage and was trapped at a minimum temperature of 160–170°C and low pressures, which correspond to maximum temperature conditions obtained from bitumen reflectance data. Subsequently, the isolated fluid system increased its salinity and was trapped in the same clear saddle dolomite crystals (rims) at lower P–T conditions (110–120°C, low pressure). Continuous brittle deformation caused post-entrapment re-equilibration of part of these fluid inclusions, resulting in partial leakage (i.e., higher T_h values). The origin of this fluid precipitating clear saddle dolomite is unclear, but Sr isotope data clearly indicate a contact of the

precipitating fluid with Paleozoic terrigenous clastics. The widespread presence of high salinity fluids in the area (Gasparrini 2003; Gasparrini et al. 2006a; Gasparrini et al. 2006b; Ayllón et al. 2003; Lapponi et al. 2004; Lapponi et al. 2005), causing volumetrically important epigenetic dolomitization farther to the north, can be taken as an argument for a widespread fluid flow at the end of the formation of clear saddle dolomite (precipitation of the outer rim zone of this cement). During this period, relatively uniform hydrochemical conditions have to be assumed. This highly saline fluid event is probably related to a thermal peak, occurring in late Stephanian and Early Permian time, when oroclinal bending was associated with crustal thinning as well as magmatism (Gutiérrez-Alonso et al. 2004). The study area forms part of the outer zone of the Cantabrian orocline, which was characterized by a predominantly extensional setting that favored fluid flow and uniform hydrochemistry but focused most of the flow along higher-permeability pathways.

The data indicate that a more open fluid system, containing a high-salinity brine, was able to enter the less porous and permeable Devonian La Vid succession for only a limited period of time and to a minor degree. Fluid flow was most effective in the higher-permeability areas outside, and had a connection with the La Vid area for only a short period. This period of connection corresponds to the orocline formation in the latest Carboniferous to Early Permian, when extension and crustal thinning caused intense fluid circulation.

The porosity and permeability of the Paleozoic rock was modified in post-Variscan time (Alpidic orogeny) as external fluids were able to flow effectively along reactivated predefined pathways, like faults. Calcite, celestite, and kaolinite precipitated out of a low-salinity aqueous solution under shallow conditions (< 50°C) in brecciated veins and the host rock (Fig. 16). Fe-rich dolomite from the first stage recrystallized and/or was partially dissolved to form Fe-oxhydroxides and calcite.

ACKNOWLEDGMENTS

The Deutsche Forschungsgesellschaft Graduiertenkolleg 273 on water–rock interaction at Heidelberg University made financial support for this study available. We thank Z. Veselovsky for providing the stratigraphic profile of the La Vid type section, K. Frings for his support in vitrinite reflectance measurements, as well as H.G. Machel and R. Stasiuk for $^{87}\text{Sr}/^{86}\text{Sr}$ analyses. We are indebted to the other members of the “Cantabrian Group” for discussion: F. Ayllón, K. Carrière, B. Dietrich, K. Frings, M. Gasparrini, J. Grimmer, F. Lapponi, and Z. Veselovsky. We also thank J. Pironon, R. Worden, and S. Zeeh for reviews, comments, and fruitful discussions of an earlier version of this paper. The final version benefited strongly from comments, and suggestions of the reviewers R. Burrus, C. Taberner, and associate editor R.H. Goldstein.

REFERENCES

- ALLER, J., 1986, La estructura del sector meridional de las unidades del Aramo y de la Cuenca Carbonífera: Consejería de Industria y Comercio, Oviedo, 180 p.
- AYLLÓN, F., BAKKER, R.J., AND WARR, L.N., 2003, Thermal decrepitation of low temperature quartz inclusions in a Stephanian pull-apart basin, Northern Spain: *Geofluids*, v. 3, p. 49–68.
- BAADSGAARD, H., CHAPLIN, C., AND GRIFFIN, W.L., 1986, Geochronology of the Glosnerneia pegmatite, Froland, Southern Norway: *Norsk Geologisk Tidsskrift*, v. 64, p. 111–119.
- BAKKER, R.J., 2003, Package FLUIDS 1. New computer programs for the analysis of fluid inclusion data: *Chemical Geology*, v. 194, p. 3–23.
- BAKKER, R.J., 2004, Raman spectra of fluid and crystal mixtures in the system H_2O , H_2O – NaCl and H_2O – Mg_2Cl at low temperatures: applications to fluid inclusion research: *Canadian Mineralogist*, v. 42, p. 1283–1314.
- BAKKER, R.J., AND DIAMOND, L., 2006, Estimation of volume fractions of liquid and vapor phases in fluid inclusions, and definition of inclusion shapes: *American Mineralogist*, v. 91, p. 635–657.
- BARKER, M., AND PAWLEWICZ, C., 1994, An empirical determination of the minimum number of measurements to estimate the mean random vitrinite reflectance of disseminated organic matter (abstract): *American Association of Petroleum Geologists and SEPME, Annual Meeting Abstracts*, 231 p.

- BRIME, C., 1985, A diagenesis to metamorphism transition in the Hercynian of NW Spain: *Mineralogical Magazine*, v. 49, part 3, p. 481–484.
- BRIME, C., GARCIA-LOPEZ, S., BASTIDA, F., VALIN, M.L., SANZ-LOPEZ, J., AND ALLER, J., 2001, Transition from diagenesis to metamorphism near the front of the Variscan regional metamorphism (Cantabrian Zone, northwestern Spain): *Journal of Geology*, v. 109, p. 363–379.
- BODNAR, R.J., 1990, Petroleum migration in the Miocene Monterey Formation, California, U.S.A.: constraints from fluid-inclusion studies: *Mineralogical Magazine*, v. 54, p. 295–304.
- BRICHHAUSEN, H., LITKE, R., AND HANTSCH, T., 2005, Mudstone compaction and its influence on overpressure generation, elucidated by a 3D case study in the North Sea: *International Journal of Earth Sciences*, v. 94, p. 956–978.
- BURRUS, R.C., 1981, Hydrocarbon fluid inclusions in studies of sedimentary diagenesis, in Hollister, L.S., and Crawford, M.L., eds., *Fluid Inclusions, Applications to Petrology*: Mineralogical Association of Canada, Short Course Handbook, v. 6, p. 138–156.
- CAREY, S.W., 1955, The oroclinal concept in geotectonics: *Royal Society of Tasmania, Proceedings*, v. 89, p. 255–288.
- DALLMEYER, R.D., AND MARTINEZ-GARCIA, E., 1990, Pre-Mesozoic Geology of Iberia: Berlin, Springer-Verlag, 416 p.
- DICKSON, J.A.D., 1965, A modified staining technique for carbonates in thin section: *Nature*, v. 205, 587 p.
- DUBESSY, J., AUDEUD, D., WILKINS, R., AND KOSZTOLANYI, C., 1982, The use of Raman microprobe mole in the determination of the electrolytes dissolved in the aqueous phase of fluid inclusions: *Chemical Geology*, v. 37, p. 137–150.
- DUBOIS, M., AND MARIGNAC, C., 1997, The H_2O - NaCl - MgCl_2 ternary phase diagram with special application to fluid inclusion studies: *Economic Geology*, v. 92, p. 114–119.
- EVERS, H.J., 1967, Geology of the Leonides between the Bernesga and Porma rivers, Cantabrian Mountains, NW Spain: *Leidsche Geologische Mededelingen*, v. 41, p. 83–151.
- FOSCOLOS, A.E., 1990, Catagenesis of argillaceous sedimentary rocks, in McIlreath, I.A., and Morrow, D.W., eds., *Diagenesis*: Ottawa, Geoscience Canada, Reprint Series 4, p. 177–187.
- FRINGS, K., LUTZ, R., DEWALL, H., AND WARR, L.N., 2004, Coalification history of the Stephanian Cifera–Matallana pull-apart basin, NW-Spain: combining anisotropy of vitritite reflectance and thermal modeling: *International Journal of Earth Sciences*, v. 93, p. 92–106.
- GALLÁSTEGUI, G., HEREDIA, N., RODRÍGUEZ-FERNÁNDEZ, L.R., AND CUESTA, A., 1990, El stock de Peña Prieta en el contexto del magmatismo de la Unidad del Pisuerga–Carrión (Zona Cantábrica, N de España): *Cuadernos do Laboratorio Xeoloxico de Laxe*, v. 15, p. 203–217.
- GASPARRINI, M., 2003, Large-scale hydrothermal dolomitisation in the southwestern Cantabrian Zone (NW-Spain): causes and controls of the process and origin of the dolomitising fluids [Ph.D. Thesis]: University of Heidelberg, Heidelberg, Germany (<http://www.ub.uni-heidelberg.de/archiv/3586>), 193 p.
- GASPARRINI, M., BECHSTÄDT, T., AND BONI, M., 2006a, Massive hydrothermal dolomitization in the Southwestern Cantabrian Zone (Spain) and its relation to the late Variscan evolution: *Marine and Petroleum Geology*, v. 23, p. 543–568.
- GASPARRINI, M., BAKKER, R.J., AND BECHSTÄDT, T., 2006b, Characterization of dolomitizing fluids in the Carboniferous of the Cantabrian Zone (NW Spain): a fluid-inclusion study with cryo-Raman spectroscopy: *Journal of Sedimentary Research*, v. 76, p. 1304–1322.
- GOLDSTEIN, R.H., AND REYNOLDS, T.J., 1994, Systematics of fluid inclusions in diagenetic minerals: SEPM, Short Course 31, 198 p.
- GRIMMER, J.O.W., 2001, Fluidassoziierte Brekzien als Monitor dolomitisierender und dedolomitisierender Lösungsströme in der Kantabrischen Zone (Nordspanien) [Ph.D. Thesis]: University of Heidelberg, Heidelberg, Germany (<http://www.ub.uni-heidelberg.de/archiv/1423>), 148 p.
- GUTIÉRREZ-ALONSO, G., FERNÁNDEZ-SUÁREZ, J., AND WEIL, A.B., 2004, Oroclinal triggered lithospheric delamination, in Sussman, A.J., and Weil, A.B., eds., *Orogenic Curvature: Integrating Paleomagnetic and Structural Analyses*: Geological Society of America, Special Paper 383, p. 121–130.
- HAGEMANN, H.W., AND HOLLERBACH, A., 1985, The fluorescence behavior of crude oils with respect to their thermal maturation and degradation: *Organic Geochemistry*, v. 10, p. 473–480.
- HANOR, J., 2000, Barite-celestite geochemistry and environments of formation, in Alpers, C.N., Jambor, J.L., and Nordstrom, D.K., eds., *Sulfate Minerals: Reviews in Mineralogy and Geochemistry*, v. 40, p. 193–275.
- IMMENHAUSER, A., KENTER, J.A.M., GANSEN, G., BAHAMONDE, J.R., VAN VLIET, A., AND SAHER, M.H., 2002, Origin and significance of isotope shifts in Pennsylvanian carbonates (Asturias, NW Spain): *Journal of Sedimentary Research*, v. 72, p. 82–94.
- JACOB, H., 1989, Classification, structure, genesis and practical importance of natural solid oil bitumen (“migrabitumen”): *International Journal of Coal Geology*, v. 11, p. 65–79.
- JULIVERT, M., 1971, Décollement tectonics in the Hercynian Cordillera of NW Spain: *American Journal of Science*, v. 270, p. 1–29.
- JULIVERT, M., AND MARCOS, A., 1973, Superimposed folding under flexural conditions in the Cantabrian Zone (Hercynian Cordillera, Northwest Spain): *American Journal of Science*, v. 273, p. 353–375.
- KELLER, M., AND GRÖTSCH, J., 1990, Depositional history and conodont biostratigraphy of the Lower Devonian La Vid Group in the Luna area (Cantabrian Mountains, NW-Spain): *Neues Jahrbuch für Geologie und Paläontologie, Monatshefte*, p. 141–164.
- KELLER, M., AND KRUMM, S., 1993, Variscan versus Caledonian and Precambrian metamorphic events in the Cantabrian Mountains, northern Spain: *Deutsche Geologische Gesellschaft, Zeitschrift*, v. 144, p. 88–103.
- LAPPONI, F., BECHSTÄDT, T., BONI, M., BAKKER, R., AND SCHNEIDER, J., 2004, Burial dolomitization in the carbonate succession of the Cambrian Lancara Fm., Cantabrian Mountains (NW Spain) (abstract): 32nd International Geological Congress, Florence, Italy, Abstract with Programs, 829 p.
- LAPPONI, F., BAKKER, R., AND BECHSTÄDT, T., 2005, Low temperature behaviour of natural fluid inclusions in dolomite (abstract): Abstract with programs e-Book, European Current Research on Fluid Inclusions XVIII, Siena, Italy.
- LAW, B.E., AND SPENCER, C.W., 1998, Abnormal pressure in hydrocarbon environments, in Law, B.E., Ulmshiek, G.F., and Slavin, V.I., eds., *Abnormal Pressure in Hydrocarbon Environments*: American Association of Petroleum Geologists, Memoir 70, p. 1–11.
- LEROY, J., 1979, Contribution à l'étalonnage de la pression interne des inclusions fluides lors de leur decapitation: *Bulletin de Minéralogie*, v. 102, p. 584–593.
- LOTZE, F., 1945, Zur Gliederung der Varisziden der Iberischen Meseta: *Geotektonische Forschung*, v. 6, p. 78–92.
- MCILMANS, R.K., 1991, Studies of reservoir diagenesis, burial history, and petroleum migration using luminescence microscopy, in Barker, C.E., and Kopp, O.C., eds., *Luminescence Microscopy and Spectroscopy: Qualitative and Quantitative Applications*: SEPM, Short Course Notes, v. 25, p. 97–106.
- MONTEL, F., 1993, Phase equilibria needs for petroleum exploration and production industry: *Fluid Phase Equilibration*, v. 84, p. 343–367.
- NÄGLER, T., 1990, Sm-Nd, Rb-Sr and common lead isotope geochemistry on fine-grained sediments of the Iberian Massif [Unpublished Ph.D. Thesis]: Federal Technical Institute of Zurich, Switzerland, 139 p.
- NADEN, J., 1996, CalcicBrine; a Microsoft Excel 5.0 add-in for calculating salinities from microthermometric data in the system NaCl - CaCl_2 - H_2O (abstract), in Brown, P.E., and Hagemann, S.G., eds., *Sixth Biennial Pan-American Conference on Research on Fluid Inclusions (PACROFI VI): Program and Abstracts*, v. 6, p. 97–98.
- PANIAGUA, A., FONTOTÉ, L., FENOLL HACH-ALI, P., FALICK, A.E., MOREIRAS, D.B., AND CORRETGE, L.G., 1993, Tectonic setting, mineralogical characteristics, geochemical signatures and age dating of a new type of epithermal carbonate-hosted, precious metal-five elements deposits: the Villamanin Area (Cantabrian Zone, Northern Spain), in Hach-ALI, P.F., Torres-Ruiz, J., and Gervilla, F., eds., *Current Research in Geology Applied to Ore Deposits*: Rotterdam, Balkema, p. 531–534.
- PÉREZ-ESTAÚN, A., BASTIDA, F., ALONSO, J.L., MARQUÍNEZ, J., ALLER, J., ÁLVAREZ-MARRÓN, J., MARCOS, A., AND PULGAR, J.A., 1988, A thin-skinned tectonics model for an arcuate fold and thrust belt: the Cantabrian Zone (Variscan Ibero-Armorican Arc): *Tectonics*, v. 7, p. 517–537.
- PÉREZ-ESTAÚN, A., AND BASTIDA, F., 1990, Structure, Cantabrian Zone, in Dallmeyer, R.D., and Martínez-García, E., eds., *Pre-Mesozoic Geology of Iberia*: Berlin, Springer, p. 55–69.
- RAVEN, J.G.M., AND VAN DER PLUIJM, B.A., 1986, Metamorphic fluids and transtension in the Cantabrian Mountains of northern Spain: an application of the conodont color alteration index: *Geological Magazine*, v. 123, p. 673–681.
- SAMSON, I., ANDERSON, A., AND MARSCHALL, D., 2003, Fluid Inclusions, Analysis and Interpretation: Mineralogical Association of Canada, Short Course 32, 374 p.
- SCHNEIDER, J., 2002, Spätdiagenetische Prozesse in den Karbonaten der unterdevonischen La Vid Gruppe, Kantabrisches Gebirge (NW-Spanien): *Gaea Heidelbergensis (CD-ROM)*, v. 12, 119 p.
- SCHNEIDER, J., BECHSTÄDT, T., AND MACHEL, H.G., 2004a, Covariance of C- and O-isotopes with magnetic susceptibility as a result of burial diagenesis of sandstones and carbonates—an example from the Lower Devonian La Vid Group, Cantabrian Zone, NW-Spain: *International Journal of Earth Sciences*, v. 93, p. 990–1007.
- SCHNEIDER, J., DEWALL, H., KONTNY, A., AND BECHSTÄDT, T., 2004b, Magnetic susceptibility variations in carbonates of the La Vid Group (Cantabrian Zone, NW-Spain) related to burial diagenesis: *Sedimentary Geology*, v. 166, p. 73–88.
- SPÖTL, C., HOUSEKNECHT, D.W., AND JAQUES, R.C., 1998, Kerogen maturation and incipient graphitization of hydrocarbon source rocks in the Arkoma Basin, Oklahoma and Arkansas: a combined petrographic and Raman spectrometric study: *Organic Geochemistry*, v. 28, p. 535–542.
- SRODON, J., 1999, Use of clay minerals in reconstructing geological processes: recent advances and some perspectives: *Clay Minerals*, v. 34, p. 27–37.
- SUÁREZ, A., BARBA, P., HEREDIA, N., AND RODRÍGUEZ FERNÁNDEZ, L.R., 1994, Mapa Geológica de la Provincia de León, España, 1:200.000: Madrid, Instituto Geológico y Minero de España.
- TAYLOR, G.H., TEICHMÜLLER, M., DAVIS, A., DIESSEL, C.F.K., LITKE, R., AND ROBERT, P., 1998, *Organic Petrology*: Berlin, Gebrüder Borntraeger, 704 p.
- THIERY, R., PIRONON, J., WALGENWITZ, F., AND MONTEL, F., 2000, PIT (petroleum inclusion thermodynamic); a new modeling tool for the characterization of hydrocarbon fluid inclusions from volumetric and microthermometric measurements: *Journal of Geochemical Exploration*, v. 69–70, p. 701–704.

- VAN DER VOO, R., STAMATAKOS, J.A., AND PARÉS, J.M., 1997, Kinematic constraints on thrust-belt curvature from syndeformational magnetization in Lagos de Valle Syncline in the Cantabrian Arc, Spain: *Journal of Geophysical Research*, v. 102, p. 105–120.
- VEIZER, J., ALA, D., AZMY, K., BRUCKSCHEN, P., BUHL, D., BRUHN, F., CARDEN, G.A.F., DIENER, A., EBNETH, S., GODDERIS, Y., JASPER, T., KORTE, C., PAWELLEK, F., PODLAHA, O.G., AND STRAUSS, H., 1999, $^{87}\text{Sr}/^{86}\text{Sr}$, $\delta^{13}\text{C}$ and $\delta^{18}\text{O}$ evolution of Phanerozoic seawater: *Chemical Geology*, v. 161, p. 59–88.
- VESELOVSKY, Z., BECHSTÄDT, T., AND ZÜHLKE, R., in press, Structural, reverse basin and forward stratigraphic modeling of the Southern Cantabrian Basin, NW-Spain: *International Association of Sedimentologist*, Special Publication.
- WEIL, A.B., VAN DER VOO, R., VAN DER PLUIJM, B.A., AND PARÉS, J.M., 2000, The formation of an orocline by multiphased deformation: a paleomagnetic investigation of the Cantabrian–Asturias arc hinge-zone (northern Spain): *Journal of Structural Geology*, v. 22, p. 735–756.
- WEIL, A.B., VAN DER VOO, R., VAN DER PLUIJM, B.A., AND PARÉS, J.M., 2001, Oroclinal bending and evidence against the Pangea megashear: the Cantabria–Asturias arc (northern Spain): *Geology*, v. 29, p. 991–994.

Received 6 March 2005; accepted 20 August 2007.